small-interfering RNAs (siRNAs) or plasmid DNAs of p63. We clearly found some CC chemokine ligands that could be regulated by p63. Among the chemokine ligands we investigated, the only one that p63 could commonly upregulate in the three epithelial cell lines we investigated was thymus and activation-regulated chemokine (TARC)/CCL17, a strong chemoattractant of $CD4^+$ T cells like memory, regulatory and type II Th as well as Th17 cells (Vestergaard and others 2000; Baekkevold and others 2005; Hirahara and others 2006; Lim and others 2008). Tissue remodeling–associated cytokines such as transforming growth factor-β (TGF-β) and epidermal growth factor (EGF) suppressed the expression of p63 of epithelial cells as under the repair process (Kurokawa and others 2006). It was of great interest that, in accordance with the downregulation of p63, cells exposed to these cytokines showed the suppression of TARC/CCL17 as expected. This may illustrate an instructive mechanism mediated by p63, by which epithelial tissues could retain $CD4^+$ T-cell populations responsible for immunomodulation ready to be mobilized at the sites of immune reactions during the physiological healing process of epithelial tissues. As TARC/CCL17 is well known to be involved in the emergence of allergic bronchitis and allergic or atopic dermatitis, our observations may lead to further understanding of the mechanisms of such immune-related disorders (Sekiya and others 2000; Campbell and others 2007; Furusyo and others 2007).

Materials and Methods

Cell lines and cell culture

Human LC817, HaCaT, and 293 epithelial cells were maintained in modified Dulbecco's modified Eagle's medium supplemented with 10% heat-inactivated bovine calf serum, 50 μg/mL streptomycin, and 100 U/mL penicillin. All cells were cultured at 37°C in a humidified atmosphere in 5%CO_2.

Antibodies and immunohistochemistry

The antibody used was a rabbit anti-p63 polyclonal antibody (H-137; Santa Cruz Biotechnology, Santa Cruz, CA, USA). The procedures for immunofluorescence have been previously described (Kikuchi and others 2004). Signals were detected under an immunofluorescence microscope (IX71, Olympus).

RT-PCR and real-time RT-PCR

Primer pairs were selected using Primer3 software on messenger RNA sequences based on the National Center for Biotechnology Information database. Sequences of the primer pairs were finally determined after reference to the original genomic organization presented in the Ensembl database (Sanger Centre), as summarized in Table 1. Real-time polymerase chain reaction (PCR) was performed as described in the manufacturer's protocol for Assays-on-Demand Gene Expression products (Applied Biosystems). To compare the levels of expression of genes, the ΔΔCT method was employed to analyze triplicate specimens (Livak and Schmittgen 2001).

Transfection of siRNAs and plasmid DNAs

Cells were cultured at a density of 2×10^5 cells/well in a 6-well plate in 2.5-mL culture medium. After 24 h, the culture medium was replaced by medium containing a complex of the siRNAs specific for p63 (B-Bridge) and Lipofectamine RNAi MAX (Invitrogen), giving a final concentration of siRNA of 20 nM following the manufacturer's instructions. After 48 h, cells were harvested to be subjected to real-time PCR analysis. As with transfection of siRNAs, cells were prepared prior to transfection. After 24 h, 250 ng of pcDNA3.1 harboring cDNA encoding p63 (pcDNA3.1-p63) was transiently transfected using Lipofectamine 2000 reagent (Invitrogen). After 48 h, cells were harvested and analyzed.

Cell stimulation

Cells were cultured at a density of 2×10^5 cells 24 h before stimulation. Then the culture medium was replaced by a medium containing 10 U/mL TGF-β (Sigma-Aldrich) or 10 U/mL EGF (Sigma-Aldrich). After 48 h total RNA was harvested from cells to be employed in subsequent real-time PCR analysis.

Results

Chemokine ligands regulated by p63 in LC817 pulmonary epithelial cells

To address the question of whether p63 was involved in the regulation of chemokines of epithelial cells, we initially established a specialized cellular state with suppressed levels of p63 by employing the siRNA technique. When the designated siRNA from a sequence encoding p63 was transiently introduced into LC817 pulmonary epithelial cells that constitutively expressed p63, it was downregulated at transcription and protein levels as well (Fig. 1A). Using these LC817 cells, reverse transcriptase (RT)-PCR analyses of CC chemokine ligands, including CCL1 to CCL28, indicated that the expression of TARC/CCL17, CCL22, CCL25, and CCL28 was likely to be upregulated by p63 (Fig. 1B). CCL5 was also under the control of p63, but was negatively regulated. A series of CXC chemokine ligands was also investigated in LC817 cells, though there were no significant changes of any type of CXC chemokine ligand, including CXC1 to CXC16 at the transcription level (Fig. 1C). Thus p63 could regulate the levels of CC chemokine ligands of CCL5, TARC/CCL17, CCL22, CCL25, and CCL28 but not CXC chemokine ligands in LC817 cells.

Chemokine ligands regulated by p63 in HaCaT epidermal cells

To evaluate the results obtained from the analysis of LC817 cells, we further examined HaCaT epidermal cells, which also endogenously expressed p63. Prior to RT-PCR analyses, it was also confirmed that HaCaT cells with the siRNAs of p63

TABLE 1. PRIMER SEQUENCES USED IN THIS STUDY.

		forward primer			*reverse primer*		
gene name	*length (bp)*	*sequence (5′–3′)*	*Tm (°C)*	*position*	*sequence (5′–3′)*	*Tm (°C)*	*position*
CCL1	163	catttgcggagcaagagatt	60.4	exon2	tgcctcagcatttttctgtg	60.0	exon3
CCL2	171	ccccagtcacctgctgttat	60.0	exon2	tggaatcctgaacccacttc	59.9	exon3
CCL3	198	tgcaaccagttctctgcatc	60.0	exon1	tttctggacccactcctcac	60.1	exon3
CCL4	211	aagctctgcgtgactgtcct	60.2	exon1	gcttgcttcttttggtttgg	59.9	exon3
CCL5	150	cgctgtcatcctcattgcta	60.0	exon1	gagcacttgccactggtgta	59.9	exon2
CCL7	179	atgaaagcctctgcagcact	60.2	exon1	ggacagtggctactggtggt	60.0	exon2
CCL8	192	aatgtcccaaggaagctgtg	60.1	exon2	gggaggttggggaaaataaa	60.0	exon3
CCL11	233	agaaaccaccacctctcacg	60.2	exon1	cacagctttctggggacatt	60.1	exon2
CCL13	245	atctccttgcagaggctgaa	60.1	exon2	agaagaggaggccagaggag	60.1	exon3
CCL14/15	214	tcccgtgttcactcatgaaa	60.1	exon3	tcagaggctcaggaggtgtt	60.0	exon4–5
CCL16	242	ctgccctgtctctccttgtc	60.0	exon1	ctcttggacccagtcgtcat	60.1	exon3
CCL17	163	cttctctgcagcacatccac	59.6	exon1	ctgccctgcacagttacaaa	59.9	exon3
CCL18	150	agctctgctgcctcgtctat	59.4	exon2	cccacttcttattggggtca	59.8	exon3
CCL19	172	atccctgggtacatcgtgag	59.8	exon2	gcttcatcttggctgaggtc	60.0	exon3
CCL20	198	tttattgtgggcttcacacg	59.6	exon2	tgggctatgtccaattccat	60.2	exon3
CCL21	220	caagcttaggctgctccatc	60.1	exon2	tcagtcctcttgcagccttt	60.1	exon3
CCL22	212	cgcgtggtgaaacacttcta	59.9	exon2	ataatggcagggaggtaggg	60.2	exon3
CCL23	173	tttgaaacgaacagcgagtg	60.0	exon3	tgtgtcccttcaccttgaca	60.1	exon4
CCL24	228	gccttctgttccttggtgtc	59.7	exon1	tgtacctctggacccactcc	60.0	exon3
CCL25	198	acaggaaggtgtgtgggaac	59.9	exon3	tactgctgctgatgggattg	59.8	exon4
CCL26	163	ggaggagtttgggagaaacc	59.9	exon2	tgtggctgtattggaagcag	59.9	exon3
CCL27	191	agcactgcctgctgtactca	59.8	exon2	tcttggtgctcaaaccactg	59.9	exon3
CCL28	188	gctgatggggattgtgactt	59.9	exon2	ccctgatgtgccctgttact	60.0	exon3
CXCL1	171	agggaattcaccccaagaac	60.2	exon2	tggatttgtcactgttcagca	60.3	exon2–3
CXCL2	172	gcagggaattcacctcaaga	60.2	exon2	ggatttgccatttttcagc	61.0	exon3–4
CXCL3	172	gcagggaattcacctcaaga	60.2	exon2	ggtgctccccttgttcagt	61.0	exon3–4
CXCL4	174	gctgctcctgccacttgt	60.2	exon1	ttcagcgtggctatcagttg	60.0	exon2–3
CXCL5	171	gcaaggagttcatcccaaaa	60.1	exon2	ttgtttccaccgtccaaaat	60.2	exon3–4
CXCL6	158	gtcctgtctctgctgtgctg	59.8	exon2	aacttgcttcccgttcttca	59.9	exon3
CXCL7	207	tcctccaccaaaggacaaac	59.9	exon1	tttcctcccatccttcagtg	60.0	exon3
CXCL8	196	gtgcagttttgccaaggagt	60.3	exon1–2	ctctgcacccagttttcctt	59.3	exon4
CXCL9	166	ttttcctcttgggcatcatc	60.0	exon1	tcaattttctcgcaggaagg	60.3	exon2
CXCL10	172	ctgtacgctgtacctgcatca	59.9	exon2	ttcttgatggccttcgattc	60.2	exon3
CXCL11	175	agaggacgctgtctttgcat	60.0	exon2	taagccttgcttgcttcgat	60.1	exon3
CXCL12	161	tcagcctgagctacagatgc	59.3	exon2	ctttagcttcgggtcaatgc	59.9	exon3
CXCL13	151	gcttgaggtgtagatgtgtcca	60.2	exon2	tgagggtccacacacacaat	59.9	exon3
CXCL14	152	aagctggaaatgaagccaaa	59.8	exon2	ttccaggcgttgtaccactt	60.6	exon3
CXCL16	160	tctccggaaacacctgagag	60.4	exon2	cacaatccccgagtaagcat	60.0	exon4
p63	163	gaaacgtacaggcaacagca	59.9	exon10	gctgctgagggttgataagc	60.0	exon11

expressed p63 to a lesser extent than control cells (Fig. 2A). As assessed by RT-PCR analyses, CCL7, TARC/CCL17, and CCL26 were upregulated by p63 in HaCaT cells (Fig. 2B). In HaCaT cells, CCL5 was also slightly upregulated and CCL25 was downregulated by p63, though p63 insignificantly affected the expression of CCL22 and CCL28. These results, except for TARC/CCL17, did not match those of LC817 cells, suggesting that the manner of p63 regulation of CC chemokine ligands probably varied by epithelial cell type. Thus TARC/CCL17 was thought to be a particular CC chemokine ligand with a mechanism of transcription regulated by p63 that might be common in usual epithelial cells.

Excess amounts of p63 induce TARC/CCL17 in 293 epithelial cells

Following these results, we next employed an alternative approach to determine whether CC chemokine ligands CCL5, CCL7, TARC/CCL17, CCL22, CCL25, CCL26, and CCL28 were regulated by p63. As 293 epithelial cells did not endogenously express p63, the cells were transiently transfected with p63 plasmids. Interestingly RT-PCR analyses of 293 cells with excess p63 demonstrated high amounts of TARC/CCL17 (Fig. 3). The levels of CCL5 and CCL26 were relatively decreased in 293 cells with excess p63. This was

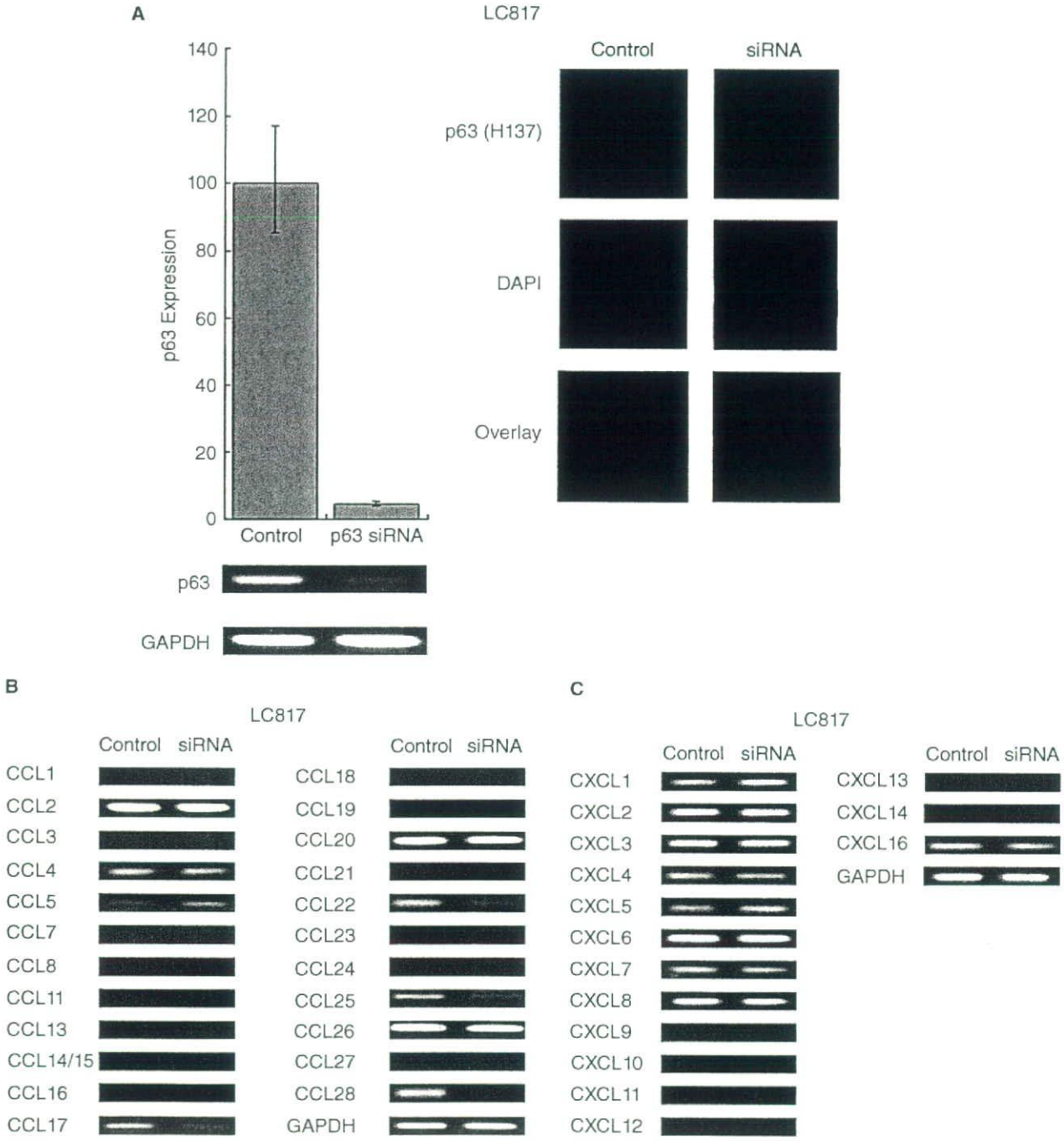

FIG. 1. Transcription analysis of LC817 pulmonary epithelial cells. (**A**) Transfection of siRNAs specific for p63 resulted in the downregulation of p63 in LC817 cells. Left panels show real-time PCR analysis of cDNAs derived from cells with siRNA specific for GFP or siRNA specific for p63. Simultaneously, cDNAs were checked by RT-PCR analysis of p63. Right panels show immunofluorescence analysis of cells with siRNA of GFP or p63 (depicted as control and siRNA, respectively), where p63 is visualized by H-137 pAb in red and the nucleus by DAPI in blue. (**B** and **C**) Transcription profiles as assessed by RT-PCR analysis of CC and CXC chemokine ligands, respectively. Control; cells transfected with GFP siRNAs, p63 siRNA or siRNA; cells with p63 siRNAs. GAPDH; a template control.

similarly found in LC817 and HaCaT cells, suggesting that p63 was probably associated with the control of the expression of CCL5 through various factors depending on the cells. In 293 cells, the levels of CCL22, CCL25, and CCL28 were not altered and CCL7 seemed not to be associated with p63. Collectively, the mechanism by which p63 positively

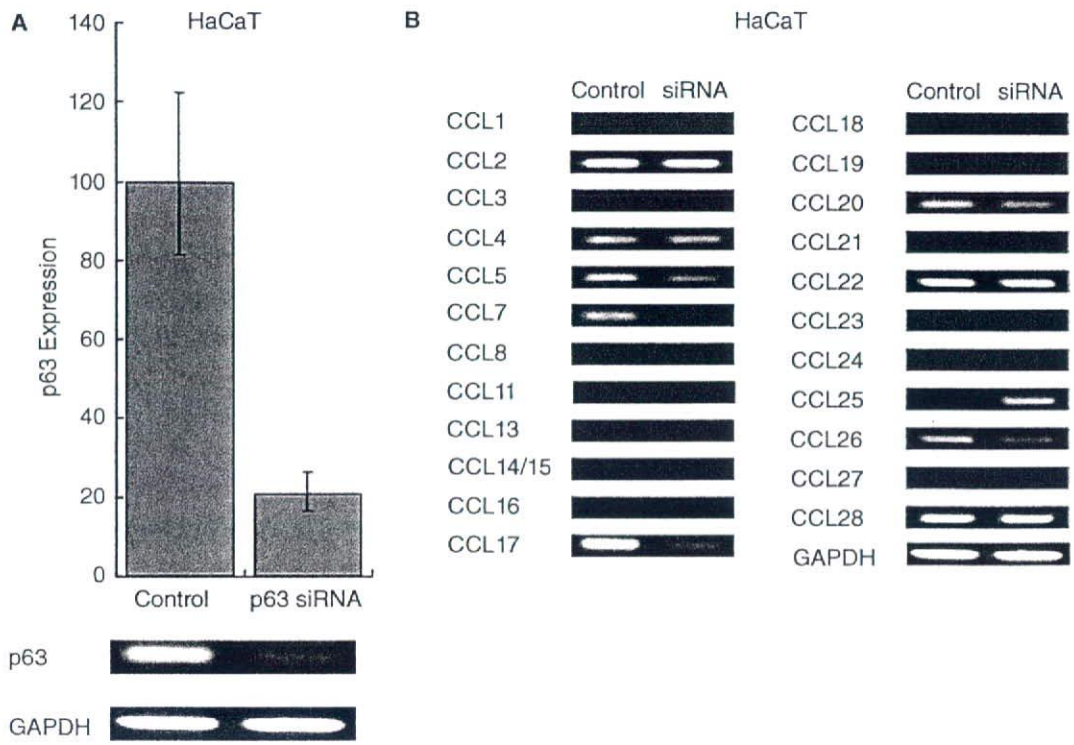

FIG. 2. Transcription analysis of HaCaT epidermal cells. (**A**) Transfection of siRNAs specific for p63 resulted in the downregulation of p63 in HaCaT cells. Real-time PCR analysis of cDNAs derived from cells with siRNA specific for GFP and with siRNA specific for p63. Simultaneously, cDNAs were evaluated by RT-PCR analysis of p63 and GAPDH as a template control. (**B**) Transcription profiles as assessed by RT-PCR analysis of CC chemikine ligands in HaCaT cells. Control; cells transfected with GFP siRNAs, siRNA; cells with p63 siRNAs. GAPDH; a template control.

induced the expression of TARC/CCL17 would generally appear to be shared by human epithelial cells. It was also observed that CCL5 and CCL26 were under the control of p63 in specific types of epithelial cells.

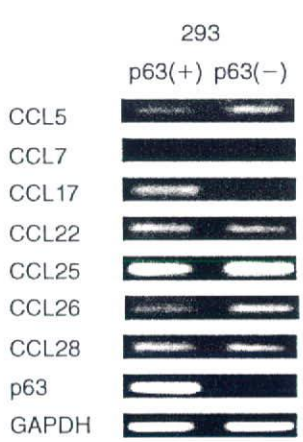

FIG. 3. Transcription analysis of CCL5, CCL7, CCL17, CCL22, CCL25, CCL26, and CCL28 in 293 epithelial cells with transiently introduced mock pcDNA3.1 or p63-pcDNA3.1 (depicted as p63(−) or p63(+), respectively) by RT-PCR. GAPDH; a template control.

TGF-β and EGF downregulate p63 and TARC/CCL17

It is well recognized that inflammatory responses are usually accompanied by inflammatory healing reactions around local epithelial tissues. A complex mechanism with multiple inflammatory cells underlays these reactions, in which TGF-β and EGF have pivotal roles in such remodeling during immune responses. When epithelial remodeling around inflammatory foci occurs, the levels of p63 are mostly suppressed in epithelial cells (Bamberger and others 2005; Kurokawa and others 2006). To examine the physiological role of p63 in the context of TARC/CCL17 expression, HaCaT cells were stimulated with TGF-β or EGF. As under inflammatory conditions, the levels of p63 were inhibited in these cells down to ~40–50% of the control levels (Fig. 4). As expected due to the downregulation of p63, the levels of TARC/CCL17 were significantly decreased to 5–10% of the control levels. This may imply physiological association of TGF-β and EGF with the regulation of TARC/CCL17 through p63.

Discussion

In this study, we first identified a role of the p63 molecule in the positive regulation of TARC/CCL17 in human

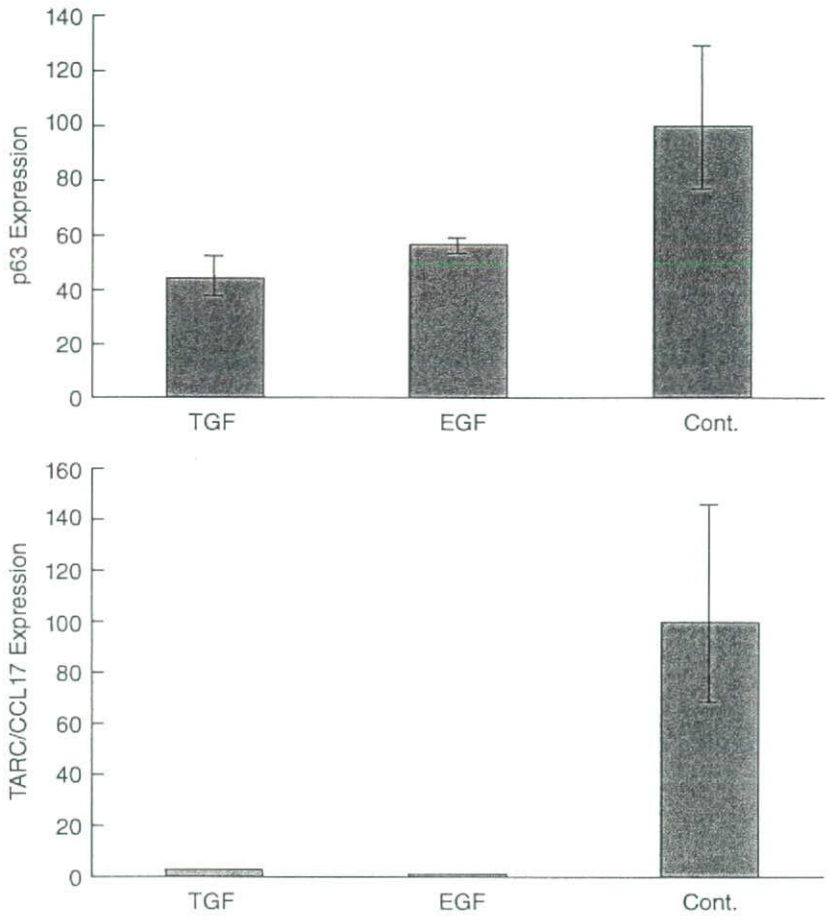

FIG. 4. Transcription analysis of p63 and TARC/CCL17 in HaCaT cells stimulated with TGF-β or EGF associated with tissue remodeling by real-time PCR. *Upper and lower panels* show levels of transcription of p63 and TARC/CCL17, respectively.

epithelial cells. The transcripts of TARC/CCL17 are exclusively detected in epithelial tissues, including lung and small and large intestines as well as thymus, suggesting that TARC/CCL17 mainly acts as a chemokine of epithelial origin (Imai and others 1996). Because p63 shows an expression profile with TARC/CCL17 in various human epithelial tissues, our results are compatible with the functional correlations implied by the expression profiles of p63 and TARC/CCL17 (Schmale and Bamberger 1997; Kikuchi and others 2004). Similar to the adhesion molecules, chemokines and their surface receptors can be up- or downregulated as cells undergo differentiation or stimulation, allowing lymphocytes to coordinate their own pathway with their immunologic functions. In this context, it is intriguing that TGF-β and EGF suppressed the levels of TARC/CCL17, probably through downregulation of p63, as during the inflammatory healing process, where external pathogens can enter into the tissues from the openings of broken epithelial cell sheets. This might imply that the p63-TARC/CCL17 axis participates in the homing and release of particular T-cell subsets and then engages efficient immune reactions at local inflammatory regions with epithelial tissue remodeling.

Since $CD4^+$ T cells chiefly conduct immunosurveillance, they have to be mobilized to the sites where antigens are localized and presented through a major histocompatibility complex or CD1 (Bendelac and others 2007). TARC/CCL17 specifically binds to the CC chemokine receptor CCR4 on the surface of the $CD4^+$ T cell. It is noteworthy that memory and regulatory T cells, Th17 and Th2 $CD4^+$ T cells, possess CCR4 and are possibly able to home through TARC/CCL17 in skin, lung, and tumor tissues (Vestargaard and others 2000; Backkevold and others 2005; Hirahara and others 2006; Lim and others 2008). Active involvement of TARC/CCL17 has also been reported in the emergence of allergic as well as atopic disorders in skin and lung (Sekiya and others 2000; Campbell and others 2007; Furusyo and others 2007). According to the Th1/Th2 paradigm, inflammation associated with allergic disorders is regarded as a Th2-dominant immune response. The cytokines liberated by allergen-reactive Th2 cells control the process leading to allergic inflammation. Thus specific control of p63 expression may lead to a new modality for the control of allergic and atopic disorders, or even cancer, through alteration of the levels of TARC/CCL17 (Ishida and Ueda 2006; Saeki and Tamaki 2006).

Previously we have reported that p63 can also activate the gene expression of human inter-cellular adhesion molecule 1 (ICAM-1), which plays a role in the binding of T cells through lymphocyte function–associated antigen-1 (LFA-1)

to epithelial cells. This mechanism may further work to enforce the affinity of epithelial cells to T cells. The promoter region of the ICAM-1 gene responsive to p63 is restricted, with a 135-bp region where an interferon-γ-activated sequence (GAS) motif, Sp-1, and AP-2 are localized (Kikuchi and others 2004). It is noteworthy that this GAS motif is seemingly shared by the proximal promoter sequence of TARC/CCL17 (Maier and others 2007). However, within a promoter sequence from 950-bp to the transcription start site of the TARF/CCL17 promoter region, we failed to find a sequence that completely matched the specific motif directly bound to p63 reported recently (Perez and others 2007). Thus it is possible to consider that p63 indirectly modulates the transactivation of the TARC/CCL17 gene through GAS or other motifs via an as yet unidentified mechanism, although more experiments will be required to determine the precise action of p63 in the regulation of these genes.

In summary, we reported novel involvement of p63 in the regulation of TARC/CCL17 of epithelial tissues under tissue repair. To respond rapidly and effectively to various immunologic insults, the coordinated action of various resident cell populations around epithelial cells as well as immigrating leukocytes enables the mucosal immune system. Our results may also shed light on the role of p63 in epithelial immune surveillance in terms of maintaining peripheral T-cell tolerance as well (Sather and others 2007).

Acknowledgments

This work was in part supported by grants-in-aid for Scientific Research (C) from JSPS (No. 20590347) and from the Akiyama Foundation to S. Ichimiya.

References

Baekkevold ES, Wurbel MA, Kivisäkk P, Wain CM, Power CA, Haraldsen G, Campbell JJ. 2005. A role for CCR4 in development of mature circulating cutaneous T helper memory cell populations. J Exp Med 201:1045–1051.

Bamberger C, Hafner A, Schmale H, Werner S. 2005. Expression of different p63 variants in healing skin wounds suggests a role of p63 in reepithelialization and muscle repair. Wound Repair Regen 13:41–50.

Bendelac A, Savage PB, Teyton L. 2007. The biology of NKT cells. Annu Rev Immunol 25:297–336.

Campbell JJ, O'Connell DJ, Wurbel MA. 2007. Cutting edge: chemokine receptor CCR4 is necessary for antigen-driven cutaneous accumulation of CD4 T cells under physiological conditions. J Immunol 178:3358–3362.

Furusyo N, Takeoka H, Toyoda K, Murata M, Maeda S, Ohnishi H, Fukiwake N, Uchi H, Furue M, Hayashi J. 2007. Thymus and activation regulated chemokines in children with atopic dermatitis: Kyushu University Ishigaki Atopic Dermatitis Study (KIDS). Eur J Dermatol 17:397–404.

Hayday A, Theodoridis E, Ramsburg E, Shires J. 2001. Intraepithelial lymphocytes: exploring the Third Way in immunology. Nat Immunol 2:997–1003.

Hirahara K, Liu L, Clark RA, Yamanaka K, Fuhlbrigge RC, Kupper TS. 2006. The majority of human peripheral blood CD4+CD25highFoxp3+ regulatory T cells bear functional skin-homing receptors. J Immunol 177:4488–4494.

Ihrie RA, Marques MR, Nguyen BT, Horner JS, Papazoglu C, Bronson RT, Mills AA, Attardi LD. 2005. Perp is a p63-regulated gene essential for epithelial integrity. Cell 120:843–856.

Imai T, Yoshida T, Baba M, Nishimura M, Kakizaki M, Yoshie O. 1996. Molecular cloning of a novel T cell-directed CC chemokine expressed in thymus by signal sequence trap using Epstein-Barr virus vector. J Biol Chem 271:21514–21521.

Ishida T, Ueda R. 2006. CCR4 as a novel molecular target for immunotherapy of cancer. Cancer Sci 97:1139–1146.

Juremalm M, Olsson N, Nilsson G. 2005. CCL17 and CCL22 attenuate CCL5-induced mast cell migration. Clin Exp Allergy. 35:708–712.

Kikuchi T, Ichimiya S, Kojima T, Crisa L, Koshiba S, Tonooka A, Kondo N, Van Der Saag PT, Yokoyama S, Sato N. 2004. Expression profiles and functional implications of p53-like transcription factors in thymic epithelial cell subtypes. Int Immunol 16:831–841.

Koster MI, Dai D, Marinari B, Sano Y, Costanzo A, Karin M, Roop DR. 2007. p63 induces key target genes required for epidermal morphogenesis. Proc Natl Acad Sci USA 104:3255–3260.

Kunkel EJ, Butcher EC. 2002. Chemokines and the tissue-specific migration of lymphocytes. Immunity 16:1–4.

Kurokawa I, Mizutani H, Kusumoto K, Nishijima S, Tsujita-Kyutoku M, Shikata N, Tsubura A. 2006. Cytokeratin, filaggrin, and p63 expression in reepithelialization during human cutaneous wound healing. Wound Repair Regen 14:38–45.

Lim HW, Lee J, Hillsamer P, Kim CH. 2008. Human Th17 cells share major trafficking receptors with both polarized effector T cells and FOXP3+ regulatory T cells. J Immunol 180:122–129.

Livak KJ, Schmittgen TD. 2001. Analysis of relative gene expression data using real-time quantitative PCR and the 2(-ΔΔ C(T)) method. Methods 25:402–408.

Maier E, Wirnsberger G, Horejs-Hoeck J, Duschl A, Hebenstreit D. 2007. Identification of a distal tandem STAT6 element within the CCL17 locus. Hum Immunol 68:986–992.

Milligan G, Smith NJ. 2007. Allosteric modulation of heterodimeric G-protein-coupled receptors. Trends Pharmacol Sci 28:615–620.

Perez CA, Ott J, Mays DJ, Pietenpol JA. 2007. p63 consensus DNA-binding site: identification, analysis and application into a p63MH algorithm. Oncogene 26:7363–7370.

Ruffini PA, Morandi P, Cabioglu N, Altundag K, Cristofanilli M. 2007. Manipulating the chemokine-chemokine receptor network to treat cancer. Cancer 15;109:2392–2404.

Saeki H, Tamaki K. 2006. Thymus and activation regulated chemokine (TARC)/CCL17 and skin diseases. J Dermatol Sci 43:75–84.

Sasaki Y, Ishida S, Morimoto I, Yamashita T, Kojima T, Kihara C, Tanaka T, Imai K, Nakamura Y, Tokino T. 2002. The p53 family member genes are involved in the Notch signal pathway. J Biol Chem 277:719–724.

Sather BD, Treuting P, Perdue N, Miazgowicz M, Fontenot JD, Rudensky AY, Campbell DJ. 2007. Altering the distribution of Foxp3+ regulatory T cells results in tissue-specific inflammatory disease. J Exp Med 204:1335–1347.

Schmale H, Bamberger C.1997. A novel protein with strong homology to the tumor suppressor p53. Oncogene 15:1363–1367.

Sekiya T, Miyamasu M, Imanishi M, Yamada H, Nakajima T, Yamaguchi M, Fujisawa T, Pawankar R, Sano Y, Ohta K, Ishii A, Morita Y, Yamamoto K, Matsushima K, Yoshie O, Hirai K. 2000. Inducible expression of a Th2-type CC chemokine thymus- and activation-regulated chemokine by human bronchial epithelial cells. J Immunol 165:2205–2213.

Truong AB, Kretz M, Ridky TW, Kimmel R, Khavari PA. 2006. p63 regulates proliferation and differentiation of developmentally mature keratinocytes. Genes Dev 20:3185–3197.

Tsukita S, Furuse M. 2000. The structure and function of claudins, cell adhesion molecules at tight junctions. Ann NY Acad Sci 915:129–135.

Vestergaard C, Bang K, Gesser B, Yoneyama H, Matsushima K, Larsen CG. 2000. A Th2 chemokine, TARC, produced by keratinocytes may recruit CLA+CCR4+ lymphocytes into lesional atopic dermatitis skin. J Invest Dermatol 115:640–646.

von Andrian UH, Mackay CR. 2000. T cell function and migration. Two sides of the same coin. N Engl J Med 343:1020–1034.

Westfall MD, Mays DJ, Sniezek JC, Pietenpol JA. 2003. The ΔNp63 phosphoprotein binds the p21 and 14–3-3s promoters in vivo and has transcriptional repressor activity that is reduced by Hay-Wells syndrome-derived mutations. Mol Cell Biol 23:2264–2276.

Address reprint requests or correspondence to:
Shingo Ichimiya, MD, PhD
Department of Pathology
Sapporo Medical University School of Medicine
Sapporo 060-8557
Japan

Tel: +81-11-611-2111 (ext. 2691)
Fax: +81-11-643-2310
E-mail: ichimiya@sapmed.ac.jp

Received 24 March 2008/Accepted 31 May 2008

SPINE Volume 33, Number 23, pp 2483–2488

Gene Expression Profile of Dorsal Root Ganglion in a Lumbar Radiculopathy Model

Hirohito Takeuchi, MD,* Satoshi Kawaguchi, MD,* Satoshi Mizuno, MD,* Takashi Kirita, MD,* Tsuneo Takebayashi, MD,* Kumiko Shimozawa, MSc,† Toshihiko Torigoe, MD,‡ Noriyuki Sato, MD,‡ and Toshihiko Yamashita, MD*

Study Design. DNA array analysis of dorsal root ganglion (DRG) using a rat model with nerve root constriction.

Objective. To determine the molecular changes in the DRG adjacent to the injured nerve root in a lumbar radiculopathy model.

Summary of Background Data. DNA array analysis in lumbar radiculopathy model has so far focused on the spinal dorsal horn. The molecular changes in the DRG adjacent to the injured nerve root in lumbar radiculopathy remain to be determined.

Methods. Bilateral L5 DRGs were removed from 12 Sprague-Dawley rats on days 2, 7, 14, and 21 after nerve root ligation and on day 7 from 3 rats with sham operation. The aRNAs from the DRGs with nerve root ligation were labeled with Cy5 dye and those from the opposite side DRG (control) were labeled with Cy3 dye, and then hybridized to a 7793-spot Panorama Micro Array. It was considered to be significantly upregulated, when an average expression ratio of Cy5 to Cy3 was 2 or more. Genes upregulated were classified into early phase group (upregulated on day 2), midphase group (upregulated on days 7 and 14), and continuous group (upregulated from day 2 to 21). Seventeen genes were subjected to validation analysis with real-time quantitative PCR.

Results. There were 16 upregulated genes in the early phase group, 56 genes in the midphase group, and 17 genes in the continuous group. Functional categorization revealed dominantly upregulated gene categories in each group; transcription/translation in the early phase group, enzyme/metabolism in the midphase group, and structure in the continuous group. Validation analysis of 17 genes demonstrated mean relative expression of 2.0 or more in all but 1 gene in the DRGs with nerve root ligation and none of them in the DRGs with sham operation.

Conclusion. The genes identified in this study, especially those involved in pain signaling and inflammation, serve as potential targets for molecular-based therapy for lumbar radiculopathy.

Key words: cDNA microarray, Sprague-Dawley rats, dorsal root ganglion, nerve root ligation, lumbar radiculopathy. **Spine 2008;33:2483–2488**

Painful lumbar radiculopathy is a common, disabling condition associating with disc herniation and spinal stenosis in the lumbar spine.[1,2] In addition to mechanical compression of nerve roots, subsequent molecular events in the adjacent dorsal root ganglion (DRG) and the dorsal horn of the spinal cord play a crucial regulatory role in the severity and chronicity of lumbar radicular pain.[3,4]

With the emergence of high-density DNA array technology, it has become possible to comprehensively investigate the levels of mRNA transcripts in tissues.[5,6] In peripheral nerve injury models, a number of DNA array studies have analyzed changes in mRNA transcripts in the DRG[7–10] and the spinal dorsal horn.[11–13] In contrast, DNA array analysis in lumbar radiculopathy model has so far focused on the spinal dorsal horn.[4,14] The molecular changes in the DRG adjacent to the injured nerve root in lumbar radiculopathy remain to be determined.

In the present study, the authors used DNA array technology in a rat model[15] to determine the gene profile in the DRG adjacent to the injured nerve root.

Materials and Methods

Animal Model

Sprague-Dawley rats (6-week-old males) were maintained in a climate-controlled room on a 12/12 hours day/night cycle and allowed free access to food and water. All animal care and experiments were carried out according to the protocol approved by the Institutional Animal Care Committee of Sapporo Medical University, Sapporo, Japan. The lumbar nerve root ligation model was developed previously in our laboratory[15] by modifying a reported model.[16] Briefly, under anesthesia with intraperitoneal injection of sodium pentobarbital (50 mg/kg body weight), the L5 lamina was removed. The left L5 nerve root was isolated and tightly ligated using a 8 to 0 nylon suture proximal to the DRG. In sham-operated rats, the right L5 nerve root was exposed by laminectomy without ligation.

Manifestation of neuropathic pain of these rats was evaluated by their susceptibility to mechanical stimuli before RNA preparation from the DRG as described previously.[15] Rats were subjected to sequential series of tactile stimulations to the plantar surface of the ipsilateral (nerve root ligated) hind paw using 12 g von Frey filaments (Stoelting, IL). The mechanical stimulus was applied to the middle area between the foot pads on the plantar surface of the left (constriction side) and right (contralateral side) hind paw. Each hind paw was probed con-

From the *Department of Orthopaedic Surgery, Sapporo Medical University School of Medicine, Sapporo, Japan; †Cancer Vaccine Laboratory, Innovation Plaza Hokkaido, Japan Science and Technology Agency, Sapporo, Japan; and ‡Department of Pathology, Sapporo Medical University School of Medicine, Sapporo, Japan.

Acknowledgment date: January 26, 2008. First revision date: April 2, 2008. Second revision date: May 11, 2008. Acceptance date: June 6, 2008.

The manuscript submitted does not contain information about medical device(s)/drug(s).

No funds were received in support of this work. No benefits in any form have been or will be received from a commercial party related directly or indirectly to the subject of this manuscript.

Address correspondence and reprint requests to Satoshi Kawaguchi, MD, Department of Orthopaedic Surgery, Sapporo Medical University School of Medicine, South 1, West 16, Chuo-ku, Sapporo 060-8543, Japan; E-mail: kawaguch@sapmed.ac.jp

secutively with 10 tactile stimulations alternating between the left and right. The trial was repeated successively 3 times with at least a 10-minute interval, which resulted in each foot receiving 30 mechanical stimulations. Mechanical sensitivity was assessed by counting the total number of withdrawal responses elicited for a total possible score of 30. Therefore, the mechanical withdrawal frequency of each rat was expressed as the number of responses obtained from the contralateral side (no constricted) was subtracted from the number of responses from the ipsilateral or constricted side. Preliminary experiments confirmed the reproducibility of pain behavior in the model. Some rats having undergone ligation of the L5 root showed plantarflexed toe deformity in the ipsilateral hind paw, which improved within 2 weeks. None of the model rats showed gait disturbance or drop foot. Subsequent to the preliminary experiments, the rats showing allodynic responses (5 times or more of subtracted withdrawals on day 2 after the operation) were elected for subsequent RNA preparation.

RNA Preparation and Labeling

Bilateral L5 DRGs were removed from rats on day 2, 7, 14, and 21 after nerve root ligation and on day 7 from sham-operated rats. Three rats were used on each day and were designated a, b, and c, respectively. They were stored at −80°C until use. Total RNAs were extracted from DRG samples with an RNeasy Mini Kit (Qiagen, Valencia, CA), according to the manufacturer's protocol. The quality of RNA was assessed by electrophoresis on 1.5% agarose gel.

Using an Amino Allyl MessageAmp aRNA Kit (Ambion, Austin, TX), total RNAs from DRGs were reverse transcribed to single-strand cDNA with the oligo-dT primer containing a T7 promoter sequence. The single-strand cDNA was then converted into a double-strand cDNA template with the T7 promoter primer. Multiple copies of amino allyl-modified aRNA were generated from the double-strand cDNA templates with aaUTP. The aRNAs from the DRGs with nerve root ligation were labeled with Cy5 dye and those from the opposite side DRG (control) were labeled with Cy3 dye.

Hybridization to cDNA Microarrays and Data Analysis

The dye-labeled aRNA samples were hybridized to a 7793-spot Panorama Micro Array (Sigma Genosys, Ishikari, Japan) for 16 hours at 45°C. One array membrane was used for each experimental rat. Intensity of Cy3 and Cy5 fluorescence for every gene spot on hybridized arrays was measured with a GenePix 4000B scanner (Axon Instrument, Austin, TX), and was analyzed with GenePix Pro 5.0 software (Axon Instrument).

For normalization, the fluorescent ratio for each spot was first log-transformed using TIGR MIDAS software, version 2.19 (The Institute for Genomic Research, Rockville, MD). Then the data for each sample were mean centered. Spots that could not be interpreted were excluded, resulting in a list of 7513 genes available for subsequent analysis. The average of expression ratio of Cy5 to Cy3 was obtained for each gene in triplicate microarray experiments (3 rats in the same experimental condition). The average ratio of 2 or more was determined as differentially expressed. Genes were classified into functional categories according to the categorization of Lacroix-Fralish *et al.*[4]

Real-Time Quantitative PCR

Seventeen genes that had been upregulated in DRG of ligated nerve roots on day 7 and also in a peripheral axotomy model in the literature[8] were picked up for validation analysis with real-time quantitative PCR. TaqMan probes for these 17 genes were designed by and purchased from Applied Biosystems (Foster City, CA). Total RNA was extracted from bilateral L5 DRGs of nerve root-ligated rats (n = 3) and sham-operated rats (n = 3) on day 7 after surgery and reverse transcribed as described earlier. For individual reactions, 1 μg of each sample cDNA was combined with 25 μL of TaqMan Universal PCR Master Mix, 2.5 μL of Inventoried Gene Expression Assay Mix including TaqMan probe, 1.5 μL of GAPDH Control Mix, and 20 μL of RNase-free water. Real-time PCR was performed with the ABI PRISM 7000 Sequence Detection system (Applied Biosystems) according to the manufacturer's protocol. All amplifications were done in triplicate and threshold cycle (C_t) scores were averaged for subsequent calculations of relative expression values. The C_t scores represent the cycle number at which fluorescence signal crosses an arbitrary threshold. The C_t scores of genes of interest for each sample were normalized against C_t scores of GAPDH. Relative expression of genes in the DRG with nerve root ligation/sham operation *versus* those in the opposite side DRG (control) was determined by the following calculation: Relative expression = $2^{-\Delta\Delta C_t}$ where $\Delta\Delta C_t$ = (C_t of ligated/sham-operated nerve DRG − C_t of GAPDH) − (C_t of control DRG − C_t of GAPDH). The mean of relative expression for each sample from 3 rats was then calculated.

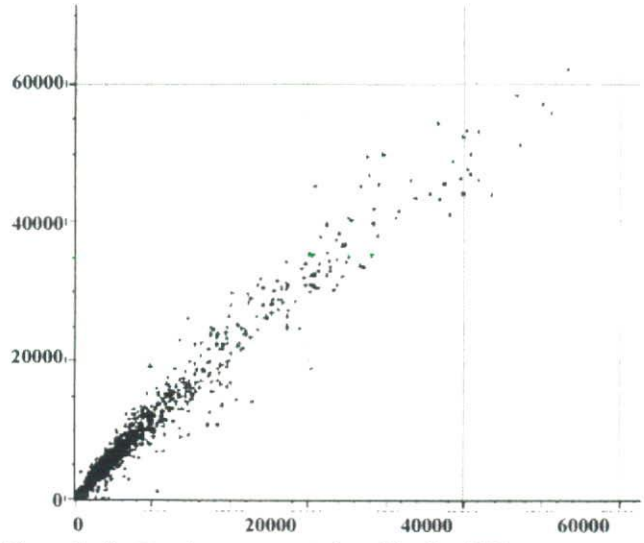

Figure 1. Scatter plot representation of lumbar DRG gene expression. Gene expression signals of the bilateral L5 DRGs in a rat 14 days after ligation of the left L5 nerve root are shown. The x-axis indicates the gene expression signals in the DRG of the ligated left L5 nerve root. The y-axis indicates the gene expression signals of the DRG of the right L5 nerve root (opposite side).

■ Results

Cluster Analysis of Gene Expression Profiles of DRG Samples

To establish gene expression profiles of a lumbar radicular pain model, we carried out cDNA array analysis on DRG sample pairs from 12 different rats with lumbar nerve root ligation and 3 rats with sham operation. As representatively shown in Figure 1, the expression of most lumbar DRG genes was not strongly changed after ligation of the nerve root. We then subjected the expression profiles of the 15 DRG sample pairs to a hierarchical

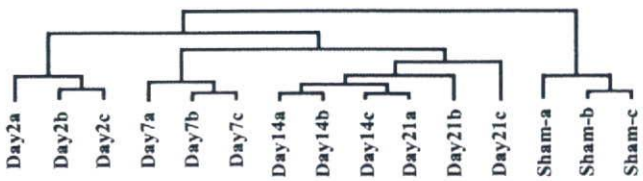

Figure 2. Hierarchial clustering of the expression profiles of 15 DRG sample pairs.

clustering analysis (Figure 2). As shown, the 3 DRG samples from sham-operated rats composed a cluster. Apart from this cluster, the 12 DRG sample pairs of nerve root-ligated rats were clustered into one large group. This group was further subdivided into 2 subgroups; 1 composed of the day-2 DRG samples, and the other composed of day-7, day-14, and day-21 samples.

Identification of Upregulated Genes in the DRG Adjacent to the Ligated Nerve Root

Based on the clustering analysis, we subsequently defined genes that were upregulated at day 2 after nerve root ligation (early phase group) and those upregulated at days 7 and 14 (midphase group). We also defined genes that were continuously upregulated from day 2 to day 21 after nerve root ligation (continuous group). As depicted in Table 1, sixteen genes were upregulated in the DRG specifically at day 2 after nerve root ligation. There were 56 genes that were upregulated both at day 7 and day 14, but not day 2 (Table 2). Seventeen genes were continuously upregulated from day 2 to day 21 after nerve root ligation (Table 3). Thus, upregulation of genes was most active in the midphase in line with the painful behavior of rats that peaked during this phase.[15]

We then classified genes into 9 functional categories. Table 4 summarizes the percentages of categorized genes in the early phase, midphase, and continuous groups. Genes categorized into cell cycle, channels/transporters, growth factors/cytokines, and synaptic represented less than 10% of the upregulated genes in all 3 groups. In contrast, 31% of genes were categorized into transcription/translation in the early phase, whereas there were 15% in the midphase and 0% in the consistent group. Inversely, more genes were involved in enzyme/metabolism and structure in the midphase and continuous groups than in the early phase group. Genes involved in signal transduction comprised 19% and 20% of the upregulated genes in the early phase and the midphase, respectively.

Validation Analysis of Array Results

Finally we evaluated the validity of array results by real-time quantitative RT-PCR. Seventeen genes were picked up from 56 genes in the midphase group. Relative expression of these genes was determined in DRGs with nerve root ligation and those with sham operation on day 7, respectively. As depicted in Table 5, all but opioid growth factor receptor showed mean relative expression of 2.0 or more in the DRGs with nerve root ligation by real-time quantitative RT-PCR. In contrast, mean relative expression of 17 genes was 1.3 or lower in the DRGs with sham operation.

■ Discussion

In the present study, we analyzed the gene expression profile of DRG neurons using a cDNA microarray in a rat nerve root ligation model. This model was used in our previous electrophysiological analysis of the DRG neurons as a lumbar radiculopathy model,[15] showing behavioral data consistent with those in the original model.[16,17] The present study was designed to extend the electrophysiological approach toward comprehensive gene profiling. We found, by cluster analysis of triplicate microarray experiments, that the gene expression profiles were distinct, with 1 set of DRG samples in sham-operated rats and another in rats having undergone nerve root ligation. In addition, among the 12 DRG samples in rats with ligated nerve roots, the 9 DRG samples taken at day 7, 14, and 21 were clustered into 1 group, apart from a

Table 1. List of DRG Genes Selectively Upregulated at Day 2 After Nerve Root Ligation

Gene Symbol	Gene Name	Accession No.	Functional Categorization	Day 2	Day 7	Day 14
Aurkb	Aurora kinase B	D89731	Cell cycle	2.2	1.6	1.5
CLCA	Putative calcium-activated chloride channel	AF077303	Channels/transporters	7.2	0.8	0.9
Ptgs2	Prostaglandin-endoperoxide synthase 2	NM_017232	Enzyme/metabolism	3.9	1.2	1.4
Hmox1	Heme oxygenase (decycling) 1	NM_012580	Enzyme/metabolism	2.6	1.6	1.1
Scgb1a1	Secretoglobin, family 1A, member 1	NM_013051	Growth factors/cytokines	2.0	1.3	1.2
Daf1	Decay accelarating factor 1	AF039584	Immune	2.1	1.4	1.6
Prlr	Prolactin receptor	L48060	Signal transduction	2.1	1.5	1.3
Nrcam	Neuron-glia-CAM-related cell adhesion molecule	U81037	Signal transduction	2.0	1.2	1.1
Flot2	Flotillin 2	AF023302	Signal transduction	2.0	1.5	1.6
Adcyap1	Adenylate cyclase activating polypeptide 1	NM_016989	Synaptic	2.8	1.6	1.4
Fosl1	Fos-like antigen 1	NM_012953	Transcription/translation	2.3	1.6	1.2
Ncl	Nucleolin	NM_012749	Transcription/translation	2.1	1.9	1.6
Rplp1	Ribosomal protein, large, P1	X15097	Transcription/translation	2.1	1.7	1.4
Pabpc1	Poly(A) binding protein, cytoplasmic 1	NM_134353	Transcription/translation	2.1	1.5	1.9
Rbm3	RNA binding motif (RNP1, RRM) protein 3	AF355190	Transcription/translation	2.0	1.8	1.5
Sval1	Seminal vesicle antigen-like 1	NM_133292	Unknown	2.0	0.7	0.8

The average Cy5/Cyt 3 ratio of gene in triplicate microarray experiments were calculated. Genes showing the ratio of 2 or more at day 2, but not at day 7 and day 14 were listed.

Table 2. List of DRG Genes Selectively Upregulated at Day 7 and Day 14 After Nerve Root Ligation

Gene Symbol	Gene Name	Accession No.	Functional Categorization	Day 2	Day 7	Day 14
S100a4	S100 calcium-binding protein A4	NM_012618	Cell cycle	1.7	3.2	2.6
Pycard	Apoptosis-associated speck-like protein containing a CARD	NM_172322	Cell cycle	1.7	2.4	2.1
Plk2	Polo-like kinase 2	AF136583	Cell cycle	1.4	2.1	2.7
Slc12a1	Solute carrier family 12, member 1	NM_019134	Channels/transporter	1.5	5.6	5.4
Aqp3	Aquaporin 3	L35108	Channels/transporter	1.3	2.7	2.9
Ctss	Cathepsin S	NM_017320	Enzyme/metabolism	1.7	4.9	3.5
Dpp6	Dipeptidylpeptidase 6	M76426	Enzyme/metabolism	1.1	4.5	4.4
Adn	Adipsin	S73894	Enzyme/metabolism	1.6	3.9	4.4
Mmp2	Matrix metallopeptidase 2	U65656	Enzyme/metabolism	1.2	3.0	2.6
Ctsk	Cathepsin K	AF010306	Enzyme/metabolism	1.4	2.7	2.4
Cnp1	Cyclic nucleotide phosphodiesterase 1	L16532	Enzyme/metabolism	1.1	2.6	2.4
Slpi	Secretory leukocyte peptidase inhibitor	AF151982	Enzyme/metabolism	1.6	2.6	2.3
Plat	Plasminogen activator, tissue	NM_013151	Enzyme/metabolism	1.5	2.5	2.6
Pld1	Phospholipase D1	U69550	Enzyme/metabolism	1.4	2.4	2.2
Cp	Ceruloplasmin	NM_012532	Enzyme/metabolism	1.2	2.4	2.2
Hspa2	Heat shock protein 2	NM_021863	Enzyme/metabolism	1.2	2.4	2.1
Xdh	Xanthine dehydrogenase	NM_017154	Enzyme/metabolism	1.4	2.4	2.4
Dnah7	Dynein, axonemal, heavy polypeptide 7	D26498	Enzyme/metabolism	1.6	2.2	2.1
Mmp10	Matrix metallopeptidase 10	M65253	Enzyme/metabolism	1.1	2.2	2.4
Ugdh	UDP-glucose dehydrogenase	AB013732	Enzyme/metabolism	1.7	2.1	2.3
Fap	Fibroblast activation protein	NM_138850	Enzyme/metabolism	1.4	2.0	2.0
Entpd2	Ectonucleoside triphosphate diphosphohydrolase 2	AF276940	Enzyme/metabolism	1.0	2.0	2.2
Mdk	Midkine	AB025023	Growth factors/cytokines	1.3	2.3	2.1
Igf1	Insulin-like growth factor I	M81184	Growth factors/cytokines	1.5	2.3	2.6
Tgfbi	Transforming growth factor, beta induced	AF305713	Growth factors/cytokines	1.5	2.2	2.0
C1qb	Complement component 1, q subcomponent, beta polypeptide	NM_019262	Immune	1.9	3.5	2.4
Cxcl9	Chemokine (C-X-C motif) ligand 9	NM_145672	Immune	1.0	3.5	3.5
Cfh	Complement component factor H	NM_130409	Immune	1.5	2.7	2.8
Cd86	Cd86 antigen	D50558	Immune	1.8	2.1	2.4
Apod	Apolipoprotein D	NM_012777	Signal transduction	1.7	4.7	3.3
Lgp85	85 kDa sialoglycoprotein	D10587	Signal transduction	1.7	3.1	2.6
Gng11	Guanine nucleotide binding protein (G protein), γ11	AF257110	Signal transduction	1.6	3.1	3.1
Gfra1	Glial cell line derived neurotrophic factor family receptor α	NM_012959	Signal transduction	1.9	3.1	2.3
Cd53	CD53 antigen	NM_012523	Signal transduction	1.7	2.8	2.3
Ramp1	Receptor (calcitonin) activity modifying protein 1	AB042887	Signal transduction	1.4	2.7	2.5
Csrp2	Cysteine and glycine-rich protein 2	U44948	Signal transduction	1.2	2.6	2.6
Ogfr	Opioid growth factor receptor	AF156878	Signal transduction	1.4	2.4	2.3
Vcam1	Vascular cell adhesion molecule 1	NM_012889	Signal transduction	1.7	2.2	2.1
Sostdc1	Uterine sensitization-associated gene 1 protein	NM_153737	Signal transduction	0.8	2.2	2.4
Slfn3	Schlafen 3	AF168795	Signal transduction	1.7	2.1	2.1
Col3a1	Collagen, type III, α1	M21354	Structure	1.8	4.0	2.9
Serpinh1	Serine (or cysteine) proteinase inhibitor, clade H, member 1	NM_017173	Structure	1.9	2.6	2.4
Lum	Lumican	X84039	Structure	1.6	2.4	2.3
Col5a1	Collagen, type V, α1	AF272662	Structure	1.5	2.3	2.5
Vil2	Villin 2	X67788	Structure	1.8	2.3	2.1
Col1a1	Collagen, type 1, α1	Z78279	Structure	1.2	2.2	2.0
DLP2	Dynein-like protein 2	D26493	Structure	1.5	2.1	2.2
Apobec1	Apolipoprotein B editing complex 1	NM_012907	Transcription/translation	1.6	3.3	3.0
Mafb	v-maf musculoaponeurotic fibrosarcoma oncogene family, protein B	U56241	Transcription/translation	1.4	2.4	2.4
Nupr1	Nuclear protein 1	AF014503	Transcription/translation	1.1	2.3	2.0
H3f3b	H3 histone, family 3B	X73683	Transcription/translation	1.6	2.2	2.0
Irf1	Interferon regulatory factor 1	NM_012591	Transcription/translation	1.7	2.1	2.0
Meox2	Mesenchyme homeo box 2	NM_017149	Transcription/translation	1.5	2.1	2.4
Btg1	B-cell translocation gene 1, anti-proliferative	L26268	Transcription/translation	1.7	2.1	2.9
Lhx2	LIM homeobox protein 2	L06804	Transcription/translation	1.6	2.0	2.4
Drcf5	Developmentally-regulated cardiac factor	U95001	Unknown	1.6	2.5	2.7

The average Cy5/Cyt 3 ratio of gene in triplicate microarray experiments were calculated. Genes showing the ratio of two or more at day 7 and day 14, but not day 2 were listed.

cluster composed of the day-2 DRG samples. Subsequently, we identified 89 genes, including 16 genes that were upregulated only at day 2 after nerve root ligation, 56 genes that were upregulated at days 7 and 14, and another 17 genes that showed consistent upregulation from day 2 to day 21. These findings indicate the involvement of distinct sets of genes in the early phase (day 2) and the later phase (day 7 and later) of development of lumbar radiculopathy. The number of upregulated genes was larger in the midphase than in the early phase, cor-

Table 3. List of DRG Genes Continuously Upregulated From Day 2 to Day 21 After Nerve Root Ligation

Gene symbol	Gene Name	Accession No.	Functional Categorization	Day 2	Day 7	Day 14	Day 21
Kif11	Kinesin family member 11	AF035955	Cell cycle	2.5	3.2	3.0	2.1
Lyz	Lysozyme	NM_012771	Enzyme/metabolism	2.1	6.2	5.0	3.6
Crabp2	Cellular retinoic acid binding protein 2	U23407	Enzyme/metabolism	3.1	3.3	3.0	2.1
Enpp3	Ectonucleotide pyrophosphatase/ phosphodiesterase 3	NM_019370	Enzyme/metabolism	2.7	3.8	4.8	2.8
Reg3g	Regenerating islet-derived 3γ	L20869	Enzyme/metabolism	2.7	2.2	4.9	2.7
A2m	α-2-macroglobulin	NM_012488	Enzyme/metabolism	5.1	11.6	10.8	2.3
Ifitm2	Interferon induced transmembrane protein 2 (1–8D)	AF164040	Immune	2.0	3.1	2.1	2.1
Gbp2	Guanylate nucleotide binding protein 2	M80367	Immune	3.1	3.9	4.1	2.1
Ifitm3	Interferon induced transmembrane protein 3	AF164039	Immune	2.3	3.3	2.6	2.3
Fcgr2b	Fc receptor, IgG, low affinity IIb	X73371	Immune	4.4	3.1	2.8	2.4
Gpnmb	Glycoprotein (transmembrane) nmb	AF184983	Signal transduction	2.3	3.6	4.8	2.9
Cdh4	Cadherin 4	D86742	Signal transduction	2.0	3.4	2.6	2.0
Vim	Vimentin	X62952	Structure	2.7	4.8	2.8	2.2
Thbs4	Thrombospondin 4	X89963	Structure	2.1	7.2	5.8	2.3
Cthrc1	Collagen triple helix repeat containing 1	NM_172333	Structure	4.7	8.7	10.4	2.5
Fn1	Fibronectin 1	NM_019143	Structure	2.8	3.3	3.1	2.1
Col18a1	Procollagen, type XVIII, α1	AF189709	Structure	3.5	6.8	5.4	2.4

The average Cy5/Cyt 3 ratio of gene in triplicate microarray experiments were calculated. Genes showing the ratio of 2 or more continuously from day 2 to day 21 were listed.

responding to the painful behavior of the nerve-ligated rats which peaked during the midphase.[15]

Functional categorization revealed dominantly upregulated gene categories in each group. They included transcription/translation, signal transduction, and enzyme/metabolism in the early phase and enzyme/metabolism, signal transduction, transcription/translation, and structure in the midphase. Consistent with our findings, genes categorized into enzyme/metabolism, signal transduction, transcription/translation, and structure were also dominantly upregulated in the dorsal horn of the spinal cord 7 and 14 days after nerve root ligation in a rat model.[4]

Based on clustering analysis, we classified genes into the early phase, midphase, and continuous group. In this regard, genes upregulated on day 14 or later may be classified as the late phase. We found only 2 genes in this group, including EGF-like domain, multiple 3 and coxsackie virus and adenovirus receptor.

Genes upregulated in the DRG with nerve root ligation may contribute to a variety of biologic processes including pain signaling, inflammation, and regeneration of the injured nerve. Of these, the genes involved in pain signaling and inflammation may serve as potential targets of pharmacological or genetic approach for lumbar radiculopathy. This idea is well exemplified by prostaglandin-endoperoxide synthase 2, which is upregulated in the early phase of our model. Prostaglandin-endoperoxide synthase 2 is known as cyclooxygenase 2 (COX-2). Involvement of COX-2 in acute pain and inflammation has been established.[18,19] Also, therapeutic efficacy of a selective COX-2 inhibitor has been demonstrated in rat radiculopathy models.[20,21] Besides prostag-

Table 4. Percentage of Genes Classified by Functional Category

	Early	Mid	Consistent
Cell cycle	6	5	6
Channels/transporters	6	4	0
Enzyme/metabolism	13	31	29
Growth factors/cytokines	6	5	0
Immune	6	7	24
Signal transduction	19	20	12
Structure	0	13	29
Synaptic	6	0	0
Transcription/translation	31	15	0
Unknown	6	2	0

Table 5. Real-Time Quantitative PCR Analysis of Day 7 DRG

Gene Name	Probe No.*	Ligation	Sham
Apolipoprotein D	Rn00562832_m1	12.0**	1.0
CD53 antigen	Rn00560957_m1	4.7	0.9
Aquaporin 3	Rn00581754_m1	64.0	0.8
Receptor (calcitonin) activity modifying protein 1	Rn00581278_m1	2.7	0.5
Secretory leukocyte peptidase inhibitor	Rn00670378_m1	15.9	0.7
Plasminogen activator, tissue	Rn00565767_m1	3.3	0.9
Heat shock protein 2	Rn00434069_s1	3.0	1.2
Xanthine dehydrogenase	Rn00567654_m1	3.9	0.9
V-maf musculoaponeurotic fibrosarcoma oncogene family, protein B	Rn00709456_s1	2.7	1.3
Opioid growth factor receptor	Rn00584280_m1	1.6	1.0
Collagen, type V, α1	Rn00593170_m1	2.6	1.0
Uterine sensitization-associated gene 1 protein	Rn00596672_m1	2.7	0.9
Polo-like kinase 2	Rn00582709_m1	3.2	1.1
cd86 antigen	Rn00571654_m1	6.4	0.9
UDP-glucose dehydrogenase	Rn00580047_m1	4.4	1.1
B-cell translocation gene 1, anti-proliferative	Rn00820872_g1	3.8	0.8
Ectonucleoside triphosphate diphosphohydrolase 2	Rn00596961_m1	3.3	1.0

*The catalog no. of TaqMan probes (Applied Biosystems).
**The mean relative expression values of three root-ligated rats and sham-operated rats were described, respectively.

landin-endoperoxide synthase 2, calcium-activated chloride channel may contribute to pain signaling in lumbar radiculopathy, because calcium-activated chloride current[22] has been shown to increase after axotomy in rats. In contrast to these molecules, heme oxygenase (decycling) 1 serves cytoprotective actions in several pathologic conditions including inflammation[23] and sciatic nerve injury.[24] Thus, there may be therapeutic benefits with heme oxygenase (decycling) 1 in lumbar radiculopathy. Among 56 genes that were upregulated in the midphase, the involvement of cathepsin S in neuropathic pain has been recently reported.[25,26] Given the fact that inhibition of cathepsin S led to reversal of neuropathic pain after peripheral nerve injury, this approach can also be applied to neuropathic condition subsequent to lumbar radiculopathy.

The present study has several limitations, including– (i) imperfect validity of microarray results (94%), (ii) placement of sham-operated controls only at 1 time point (day 7), and (iii) lack of immunohistochemical or *in situ* hybridization studies that reveals cell types expressing genes upregulated. Nevertheless, this is the first comprehensive analysis of gene expression in the DRG adjacent to nerve root ligation. The present study serves as the initial step toward identification of therapeutic targets for lumbar radiculopathy and development of molecularly targeted therapy.

■ Key Points

- DNA array analysis was conducted for the DRG adjacent to the injured nerve root in a rat lumbar radiculopathy model.
- Of 7793 genes analyzed, 16 genes were upregulated in the DRG on day 2 after nerve root ligation (early phase group), 56 genes on both days 7 and 14 (midphase group), and 17 genes from day 2 to day 21 (continuous group).
- Dominantly upregulated gene categories were transcription/translation in the early phase group, enzyme/metabolism in the midphase group, and structure in the continuous group.

References

1. Hasue M. Pain and the nerve root: an interdisciplinary approach. *Spine* 1993;18:2053–305.
2. Winkelstein BA, DeLeo JA. Mechanical thresholds for initiation and persistence of pain following nerve root injury: mechanical and chemical contributions at injury. *J Biomech Eng* 2004;126:258–63.
3. Song XJ, Vizcarra C, Xu DS, et al. Hyperalgesia and neural excitability following injuries to central and peripheral branches of axons and somata of dorsal root ganglion neurons. *J Neurophysiol* 2003;89:2185–93.
4. Lacroix-Fralish ML, Tawfik VL, Tanga FY, et al. Differential spinal cord gene expression in rodent models of radicular and neuropathic pain. *Anesthesiology* 2006;104:1283–92.
5. Reilly SC, Cossins AR, Quinn JP, et al. Discovering genes: the use of microarrays and laser capture microdissection in pain research. *Brain Res Brain Res Rev* 2004;46:225–33.
6. Zhang X, Xiao HS. Gene array analysis to determine the components of neuropathic pain signaling. *Curr Opin Mol Ther* 2005;7:532–7.
7. Costigan M, Befort K, Karchewski L, et al. Replicate high-density rat genome oligonucleotide microarrays reveal hundreds of regulated genes in the dorsal root ganglion after peripheral nerve injury. *BMC Neurosci* 2002;3:16.
8. Xiao HS, Huang QH, Zhang FX, et al. Identification of gene expression profile of dorsal root ganglion in the rat peripheral axotomy model of neuropathic pain. *Proc Natl Acad Sci USA* 2002;99:8360–5.
9. Valder CR, Liu JJ, Song YH, et al. Coupling gene chip analyses and rat genetic variances in identifying potential target genes that may contribute to neuropathic allodynia development. *J Neurochem* 2003;87:560–73.
10. Rodriguez Parkitna J, Korostynski M, Kaminska-Chowaniec D, et al. Comparison of gene expression profiles in neuropathic and inflammatory pain. *J Physiol Pharmacol* 2006;57:401–14.
11. Ko J, Na DS, Lee YH, et al. cDNA microarray analysis of the differential gene expression in the neuropathic pain and electroacupuncture treatment models. *J Biochem Mol Biol* 2002;35:420–7.
12. Sun H, Xu J, Della Penna KB, et al. Dorsal horn-enriched genes identified by DNA microarray, in situ hybridization and immunohistochemistry. *BMC Neurosci* 2002;3:11.
13. Yang L, Zhang FX, Huang F, et al. Peripheral nerve injury induces transsynaptic modification of channels, receptors and signal pathways in rat dorsal spinal cord. *Eur J Neurosci* 2004;19:871–83.
14. LaCroix-Fralish ML, Tawfik VL, Spratt KF, et al. Sex differences in lumbar spinal cord gene expression following experimental lumbar radiculopathy. *J Mol Neurosci* 2006;30:283–95.
15. Kirita T, Takebayashi T, Mizuno S, et al. Electrophysiologic changes in dorsal root ganglion neurons and behavioral changes in a lumbar radiculopathy model. *Spine* 2007;32:E65–72.
16. Hashizume H, DeLeo JA, Colburn RW, et al. Spinal glial activation and cytokine expression after lumbar root injury in the rat. *Spine* 2000;25:1206–17.
17. Abe M, Kurihara T, Han W, et al. Changes in expression of voltage-dependent ion channel subunits in dorsal root ganglia of rats with radicular injury and pain. *Spine* 2002;27:1517–24; discussion 25.
18. Lee Y, Rodriguez C, Dionne RA. The role of COX-2 in acute pain and the use of selective COX-2 inhibitors for acute pain relief. *Curr Pharm Des* 2005;11:1737–55.
19. Bingham S, Beswick PJ, Blum DE, et al. The role of the cylooxygenase pathway in nociception and pain. *Semin Cell Dev Biol* 2006;17:544–54.
20. Deleo TA, Hashizume H, Rutkowski MD, et al. Cyclooxygenase-2 inhibitor SC-236 attenuates mechanical allodynia following nerve root injury in rats. *J Orthop Res* 2000;18:977–82.
21. Kawakami M, Matsumoto T, Hashizume H, et al. Epidural injection of cyclooxygenase-2 inhibitor attenuates pain-related behavior following application of nucleus pulposus to the nerve root in the rat. *J Orthop Res* 2002;20:376–81.
22. Andre S, Boukhaddaoui H, Campo B, et al. Axotomy-induced expression of calcium-activated chloride current in subpopulations of mouse dorsal root ganglion neurons. *J Neurophysiol* 2003;90:3764–73.
23. Li C, Hossieny P, Wu BJ, et al. Pharmacologic induction of heme oxygenase-1. *Antioxid Redox Signal* 2007;9:2227–39.
24. Hirata K, He JW, Kuraoka A, et al. Heme oxygenase1 (HSP-32) is induced in myelin-phagocytosing Schwann cells of injured sciatic nerves in the rat. *Eur J Neurosci* 2000;12:4147–52.
25. Barclay J, Clark AK, Ganju P, et al. Role of the cysteine protease cathepsin S in neuropathic hyperalgesia. *Pain* 2007;130:225–34.
26. Clark AK, Yip PK, Grist J, et al. Inhibition of spinal microglial cathepsin S for the reversal of neuropathic pain. *Proc Natl Acad Sci USA* 2007;104:10655–60.

Downregulation of *Tie2* gene by a novel antitumor sulfolipid, 3′-sulfoquinovosyl-1′-monoacylglycerol, targeting angiogenesis

Yoko Mori,[1] Hiroeki Sahara,[1,5] Kayo Matsumoto,[1] Nobuaki Takahashi,[1] Takayuki Yamazaki,[3] Keisuke Ohta,[3] Satoko Aoki,[3] Masahiko Miura,[4] Fumio Sugawara,[3] Kengo Sakaguchi[3] and Noriyuki Sato[2]

[1]Marine Biomedical Institute, [2]Department of Pathology, Sapporo Medical University School of Medicine, S1, W17, Chuo-ku, Sapporo 060-8556; [3]Department of Applied Biological Science, Frontier Research Center for Genomic Drug Discovery, Tokyo University of Science, 2641 Yamazaki, Noda, Chiba 278-8510; [4]Oral Radiation Oncology, Department of Oral Restitution, Graduate School, Tokyo Medical and Dental University, Yushima, Bunkyo-ku, Tokyo, Japan

(Received October 12, 2007/Revised January 7, 2008; January 15, 2008/Accepted January 21, 2008/Online publication March 28, 2008)

We previously reported that 3′-sulfoquinovosyl-1′-monoacylglycerol (SQMG) was effective in suppressing the growth of solid tumors due to hemorrhagic necrosis *in vivo*. In the present study, we investigated the antiangiogenic effect of SQMG. *In vivo* assessment of antitumor assays showed that some tumor cell lines, but not others, were sensitive to SQMG. Microscopic study suggested that in SQMG-sensitive tumors, but not SQMG-resistant tumors, angiogenesis was reduced. We next investigated gene expression relating to angiogenesis in tumor tissues by quantitative real-time polymerase chain reaction. Consequently, although vascular endothelial growth factor gene expression was not detected with significant differences among the cases, significant downregulation of *Tie2* gene expression was observed in all SQMG-sensitive tumors as compared with controls, but not in SQMG-resistant tumors. These data suggested that the antitumor effects of SQMG could be attributed to antiangiogenic effects, possibly via the downregulation of *Tie2* gene expression in SQMG-sensitive tumors. (*Cancer Sci* 2008; 99: 1063–1070)

Angiogenesis, the formation of new blood vessels, is a fundamental process required for normal embryonic development and for the development of pathological conditions such as cancer.[1,2] Its importance in solid tumor growth and metastasis has been widely recognized by multiple studies.[2] Therefore, antiangiogenic treatments may be a promising target for the treatment of cancer. For example, it was reported that agents such as angiostatin, endostatin, and anti-vascular endothelial growth factor (VEGF) antibodies that inhibited VEGF receptor tyrosine kinase were developed, resulting in effective inhibition of solid tumor growth *in vivo*.[3–9] However, it was reported that the receptor tyrosine kinase Tie2 could play a critical role in tumor-induced angiogenesis.[10,11] It was also demonstrated that the suppression of Tie2 signaling caused by using specific blocking agents such as soluble dominant-negative receptors,[11–14] an antisense oligonucleotide,[15] RNA aptamers and RNA interference,[16,17] and a short synthetic peptide[18] resulted in antitumor effects by influencing anti-angiogenesis. Thus, therapeutic antiangiogenesis for cancer treatment using multiple strategies was reported and its importance has been widely recognized as a promising treatment for cancer chemotherapy. However, there are few reports about chemotherapeutic compounds for cancer targeting Tie2.

We previously reported that the growth of human adenocarcinoma tumors treated with 3′-sulfoquinovosyl-1′-monoacylglycerol (SQMG) was inhibited, and these tumors showed extensive hemorrhagic necrosis by pathohistological examination.[19,20] However the mechanism by which hemorrhagic necrosis occurs via the antiangiogenesis activity of SQMG remains undefined. Recently, Sakimoto *et al.* reported that combined treatment with α-SQMG (C18:0) and radiation synergistically inhibited the growth of human tumors transplanted into nude mice, accompanied by a significant reduction in the vascularity of the tumors.[21] Here, we demonstrate that the antitumor effects of SQMG could be attributed to inhibition of tumor antiangiogenesis, which seems to be involved in downregulation of the *Tie2* gene. Thus, SQMG is a promising candidate as an antitumor drug targeting angiogenesis.

Materials and Methods

Synthesis of SQMG. The chemical structure of the synthesized compound SQMG containing fatty acid 18:1 (oleic acid C18:1) is shown in Figure 1. The procedure for synthesis of SQMG was described previously.[20]

Cell lines. Human breast adenocarcinoma MDA-MB-231, lung adenocarcinoma A549, colon adenocarcinoma WiDr, prostate adenocarcinoma PC-3, tongue squamous cell carcinoma SAS, esophagus squamous cell carcinoma TE-8, lung small cell carcinoma LU65 lines, and mouse normal fibroblast NIH3T3 were used in the present study. MDA-MB-231, A-549, WiDr, PC-3, and NIH3T3 were provided by the Japanese Cancer Research Resources Bank. SAS, Lu65, and TE-8 cells were obtained from Health Science Research Resources Bank (Sendai, Japan). A549, WiDr, PC-3, SAS, TE-8, and Lu65 cells were cultured with RPMI1640 supplemented with 10% fetal calf serum, 200 U/mL penicillin, 200 μg/mL streptomycin, and 2 mM L-glutamine. MDA-MB-231 was cultured with Leibovitz's L15 supplemented with 10% fetal calf serum, 200 U/mL penicillin, 200 μg/mL streptomycin, and 2 mM L-glutamine. Human umbilical vein endothelial cells (HUVEC) were purchased from Cambrex (Walkerville, MD, USA) and maintained according to the provider's instructions. Cells in passage numbers three to five were used for this study.

***In vivo* assessment of antitumor assay.** Inbred mice, female BALB/c nu/nμ mice (20–22 g, 7 weeks of age) were obtained from Japan SLC (Shizuoka, Japan). All procedures were carried out in compliance with the guidelines of the Animal Research Center of Sapporo Medical University. Human tumor cells from lines MDA-MB-231, A549, WiDr, PC-3, SAS, TE-8, and LU65 (10^6 cells/mouse) suspended in phosphate-buffered saline (PBS) were injected subcutaneously into a dorsal side of the mice. After implantation, the tumor sizes in all of these mice were measured at 2-day intervals. When the solid tumors grew to 30–40 mm^3 in tumor volume (tumor volume = length × [width]^2

[5]To whom correspondence should be addressed.
E-mail: hsahara@sapmed.ac.jp.

doi: 10.1111/j.1349-7006.2008.00785.x

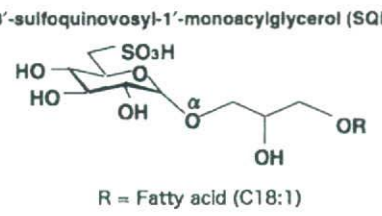

Fig. 1. Structure of 3'-sulfoquinovosyl-1'-monoacylglycerol (SQMG). SQMG contains a single fatty acid, R = C18:1.

× 0.5), SQMG was administrated every day for 14 days, and the tumor growth was observed. Each type of tumor was divided randomly into two or three groups (n = 4/group). A control group was injected intraperitoneally with 0.2 mL saline solution, and test groups were injected intraperitoneally with SQMG at a dose of 5 or 20 mg/kg every day for 14 days. On the next day after the last administration of SQMG, the tumor size was measured, and tumors were excised and prepared for further study. The mean ± SE tumor volume from each group (n = 4/group) is shown (Fig. 2). The growth of each tumor was analyzed using Student's t-test.

Immunohistochemical study. All tumors excised from mice (n = 4/group) were embedded in Tissue-Tek OCT Compound (Sakura Finetek USA, Torrance, CA, USA) and frozen. Acetone-fixed cryosections were stained with an antimouse CD31 monoclonal antibody, and then antirat IgG conjugated with AlexaFlour 488 (BD Bioscience Pharmingen, CA, USA) as a secondary antibody. Nuclei were counterstained with propidium iodide (PI) (Vector Laboratories, Burlingame, CA, USA). The CD31-positive ring-form blood vessels in 500-mm^2-section areas of these samples were counted at ×100 magnification under a fluorescence microscope (Olympus AX80; Olympus, Tokyo, Japan) and is represented as the mean ± SE of four section areas from each group. The results were analyzed using Student's t-test.

3-(4,5-Dimethylthiazol-2-yl)-2,5-diphenylthtrazolium bromide assay and annexin V labeling assay. To investigate the cytotoxicity of SQMG, the 3-(4,5-dimethylthiazol-2-yl]-2,5-diphenylthtrazolium bromide (MTT) assay was carried out using HUVEC and NIH3T3 cells according to methods described previously.[19,20] Briefly, cells (5×10^3 cells/well) were cultured in 96-well plates for 24 h and then various amounts of SQMG suspended in PBS were added to the wells. Following cultivation for 48 h, 50 μg MTT was added to cells and incubation was continued for 3 h. Then 4% HCl in 2-propanol was added to each well and mixed by pipette to disrupt the cells. The absorbance of each well was measured using a multiwell scanning photometer (Micro ELISA MR600; Dynatech Laboratories, Alexandria, VA, USA) at a wavelength of 570 nm. Results were represented as the mean ± SE of triplicate wells in one of three independent experiments. The annexin V labeling assay was carried out for detection of apoptotic HUVEC. HUVEC (10^6 cells) cultured in six-well plates for 48 h in the presence or absence of various amounts of SQMG were suspended in PBS. Following cultivation, cells were double-stained with annexin-V–fluorescein and PI using the Annexin-V-FLUOS staining kit according to the manufacturer's instructions (Roche Applied Science, Penzberg, Germany). The percentage of apoptotic (annexin V and PI double positive) cells was determined by flow cytometric analysis (FACS Calibur and Cell Quest software; BD Bioscience). The results are represented as the mean ± SE of three independent experiments.

Angiogenesis assay. The angiogenesis assay was done using an Angiogenesis Kit (Kurabo, Osaka, Japan) according to the manufacturer's instructions. Briefly, HUVEC grown on human diploid fibroblast sheets on Matrigel (Kurabo, Osaka, Japan) were cultured with or without SQMG at the indicated concentrations in growth medium containing 10 ng/mL VEGF-A for 14 days. Fresh growth medium with or without SQMG was replaced 4, 7, and 9 days after incubation. After incubation, cells were fixed in 70% ethanol and immunostained with an anti-CD31 antibody for 1 h and detected using the alkaline phosphate method. The tube-formation areas of HUVEC were quantitated using Image ++ software downloaded from the internet (http://www.pluto.dti.ne.jp/~horie-ms/index-j.html). The results are represented as the mean ± SE of five independent areas. In some experiment, HUVEC grown on human diploid fibroblast sheets on Matrigel were cultured for 14 days, and then in the presence or absence SQMG for 2 days. Subsequently, the cell-derived total RNA was harvested and quantitated for the amount of mRNA copy of human VEGF receptor-1 (Flt-1), VEGF receptor-2 (KDR), and Tie2 by quantitative real-time reverse transcription (RT)–polymerase chain reaction analysis (PCR).

Quantitative real-time RT-PCR analysis. Tumor-derived total RNA was prepared using an RNeasy Mini Kit (Qiagen, Hilden, Germany) according to the manufacturer's instructions and then reverse transcribed to cDNA with a Transcriptor First Strand cDNA Synthesis Kit (Roche Applied Science). Measurement of gene expression by quantitative analysis was carried out using a LightCycler system (Roche Applied Science). Primers and hybridization probes were synthesized by Nihon Gene Research Laboratory (Sendai, Japan). Quantitative real-time RT-PCR analysis of human $VEGF_{165}$, mouse angiopoitin-1 (*Ang1*), mouse angiopoitin-2 (*Ang2*), human *Flt-1*, human *KDR*, human *Tie2*, human *CD31*, and human glucose-6-phosphate dehydrogenase (*G6PDH*) gene expression was carried out using a LightCycler FastStart DNA Master^{PLUS} SYBR Green I system (Roche Applied Science) with primer sets described in Table 1. Detection of gene expression of mouse *Flt-1*, VEGF receptor-2 (*Flk-1*), *Tie1*, *Tie2*, *CD31*, *SM22α*, and *G6PDH* was carried out using a LightCycler FastStart DNA Master HybProbe system (Roche Applied Science) with primer sets and probes described in Table 1. PCR amplification of the housekeeping gene *G6PDH* was carried out for each sample as a control for sample loading and to allow normalization among samples. To determine the absolute copy number of the target transcripts, the amplified fragments of *G6PDH* or target genes amplified by PCR using the above-described primer sets were constructed using the pCR4-TOPO cloning vector (Invitrogen, Carlsbad, CA, USA), and the concentrations of these purified plasmids were measured. The absorbance at 260 nm and copy numbers were calculated from the concentrations of samples. A standard curve was created by plotting the threshold cycle versus the known copy number for each plasmid template in the dilutions. The copy numbers for all unknown samples were determined according to the standard curve using LightCycler software 3.5.3 (Roche Applied Science). To correct differences in both RNA quality and quantity between samples, each target gene was first normalized by dividing the copy number of the target by the copy number of *G6PDH* (copy number of target/copy number of *G6PDH* = normalized target gene). The initial value corrected for the amount of *G6PDH* was indicated as 100% to evaluate the sequential alteration of the mRNA expression level. For mouse genes, each sample was corrected with the copy number of the murine *CD31* or *SM22α* gene as markers for endothelial cells and pericytes, respectively.[22,23] Thus, this represents the amount of target gene expression in an endothelial cell or pericyte, not in a human tumor cell. Results were represented as the mean ± SE of four RNA samples from each group (n = 4/group), and analyzed using Student's t-test.

Results

In vivo assessment of antitumor effects of SQMG. Seven human tumor cell lines, MDA-MB-231, A549, WiDr, PC-3, SAS,

doi: 10.1111/j.1349-7006.2008.00785.x

Table 1. Primer and probe for quantitative real-time reverse transcription–polymerase chain reaction

Gene	Forward primer (5′–3′)	Reverse primer (5′–3′)	5′ LCRed640 probe (5′–3′)	3′ Fluorescein probe (5′–3′)
Mouse Flt-1	GGCTTTGCAGATCCACAT	GCAGAGTGCTAGTGTCCAG	TCCAGGCTCATGAATTTGAAAGCGTTTACAT	TCGGTGAAAGCTCCTCAAAGGTTTTGATTCT
Mouse Flk-1	AAGCGGGACGAGGAGAGA	CCCATGTGGACCGATGTT	AAGCTTGTACCACGTGAGGTTCTCAAACG	ATTTCTGTCTGCAGTGCACACAACAGGGACA
Mouse Tie1	GAAGGAGGAGAAGGAGGCT	CAGGAAACCATCACCGGA	CAGCAAAGGCTCAGGACAGTCAGTAGTCAT	ACGTGCCAGCTCTCTAGCCAGGGCT
Mouse Tie2	CGGACTGACTACGAGCTGT	GTTGTTGCAGGGATCGC	CTCTTGGAGGAGGGAGTCCGATAGACG	TGTTGTAAATCGTCTCACAGGCCCAGGA
Mouse CD31	CACCTTATGAAAGCAAAGAG	AATCACAACTTCATCCACTG	TGTTGCTGGGTCATTGGAGGTCACCT	TTCCATGTCTCTGGTGGGCTTATCTGTGA
Mouse SM22α	GGAGATCCCAACTGGTTTATG	AGAGCTGTCAGG GCTAAGAAC	GAGGGGAAGCACGTCATTGGCCTT	AGAGGGACTTCACAGACAGCCAACTGCA
Mouse G6PDH	GCACAAGATTGATCGAGA	GAGGCAGAGTATAGATGGTGTA	CTTGTAGGTACCCTCGTACTGGAAGCCCA	TCTCTTCATCAGCTCATCTGCCTCTGTGG
Mouse Ang1	GCATCTGGAGCATGTGATG	TAGCAGTTGTATTTCAAGTCG		
Mouse Ang2	GAAGAGCGTGGACAGCACAGG	GAGTCGTCGTAGTCGAGGGG		
Human $VEGF_{165}$	AGAGCAAGACAAGAAAATCC	TACAAACAAATGCTTTCTCC		
Human Flt-1	GACTGACAGCAAACCCAAG	AGCGTGGTCGTAGGTGAAC		
Human KDR	TGGTCTCTCTGGTTGTGTATG	AAGGGTATGGGTTTGTCACTG		
Human Tie2	CAAACCCGTTAATCACTATG	TCCGATAGAAGCTGTTGTG		
Human CD31	CAACTTTTAAAAACAAGTAA	AATCTGGACCTCATCCACCG		
Human G6PDH	CTGCGTTATCCTCACCTTC	CGGACGTCATCTGAGTTG		

TE-8, and LU65, were injected subcutaneously into mice, and then these mice bearing solid tumors that grew to 30–40 mm^3 in tumor volume were injected intraperitoneally with saline or SQMG every day for 14 days. As shown in Figure 2, SQMG treatment of mice bearing MDA-MB-231, A549, WiDr, and SAS solid tumors, injected with 5 and 20 mg/kg SQMG showed significant inhibition of tumor growth as compared with the control group on the next day after the last injection date. None of the mice showed any significant loss of bodyweight throughout the experiment period (data not shown). In contrast, mice bearing PC-3, TE-8, and LU65 solid tumors injected with SQMG did not show tumor growth inhibition as compared with the control on the day after the last injection. These data demonstrate that four tumor lines, MDA-MB-231, A549, WiDr, and SAS, were sensitive to SQMG (SQMG-sensitive), but three lines, PC-3, TE-8, and LU65 were resistant (SQMG-resistant).

Antiangiogenesis activity of SQMG *in vivo*. We previously indicated that SQMG treatment results in hemorrhagic necrosis in tumors. To investigate the mechanism of the antitumor effects of SQMG, we first carried out immunohistochemical analysis to determine the angiogenesis profiles in tumors. Tumors were excised from mice on the next day after the last injection and cryosections of these acetone-fixed tumors were stained with antimouse CD31 monoclonal antibody as an endothelial cell marker. Representative photos showing immunohistochemical staining of MDA-MB-231 tumors treated with or without SQMG are presented in Figure 3, in which CD31-positive ring-form blood vessels are clearly observed for both the control (Fig. 3a,b) and SQMG treatment (Fig. 3c,d). Therefore, the CD31-positive ring-form blood vessels of all samples in 500-mm^2-section areas were counted under a fluorescence microscope. Consequently, as shown in Table 2, in all four SQMG-sensitive tumors treated with 20 mg/kg SQMG, the numbers of blood vessels were significantly decreased ($P < 0.01$) with SQMG treatments, as compared with controls. In contrast, in all three of the SQMG-resistant tumors treated with 20 mg/kg SQMG, there were no significant differences in the number of blood vessels between controls and SQMG treatments. These data suggested that the antitumor effect of SQMG could be attributed to the inhibition of tumor angiogenesis.

Inhibitory effect of SQMG on endothelial cell-derived capillary formation *in vitro*. To investigate whether SQMG directly affected the growth profile of endothelial cells, we assessed proliferation and cytotoxicity by using the human endothelial cell line HUVEC. SQMG was added to HUVEC in concentrations from 0 to 100 μM, and cell proliferation and apoptosis were analyzed using the MTT assay and annexin V labeling assay, respectively. As shown in Figure 4a, there was no obvious the inhibitory effect on the proliferation of HUVEC up to the concentration of 25 μM. When 50 or 100 μM SQMG was added to cells, the cell proliferation was inhibited to 71.5 ± 5.6 or 55.3 ± 4.5%, respectively. Meanwhile, when SQMG at concentrations from 0 to 50 μM was added to cells, 8.5–13.3% of cells were observed to be apoptotic. However, when 100 μM SQMG was added to cells, apoptotic effects were increased to 33.8 ± 11.6%, suggesting that there was minimal weak influence on the apoptosis of HUVEC up to the concentration of 50 μM SQMG (Fig. 4b).

We further considered that it would be important to evaluate the antiangiogenic activity of SQMG using an angiogenesis model *in vitro* that is considered to closely represent *in vivo* situations. It is well known that HUVEC cocultured with fibroblast cells on Matrigel form capillary networks with tube-like structures and adopt characteristics of newly formed blood vessels.[21] Before investigating the influence of SQMG on the formation of these structures, we studied fibroblast cell proliferation and cytotoxicity using mouse NIH3T3 instead of human normal fibroblasts by MTT assay. Consequently, there was no obvious

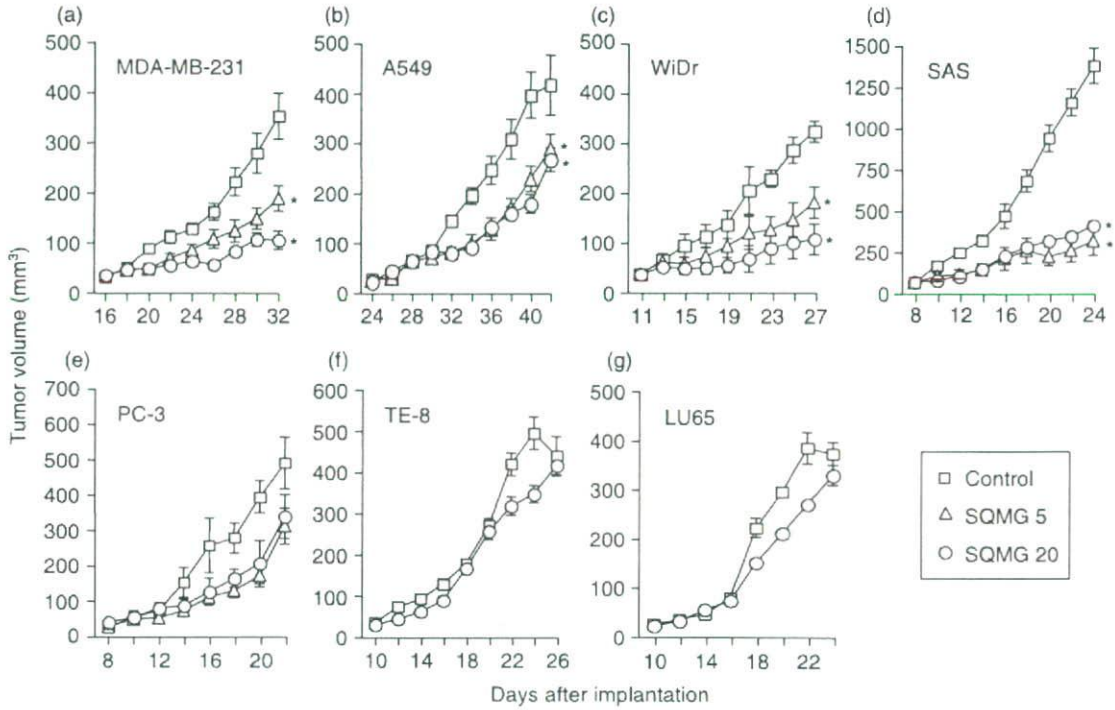

Fig. 2. *In vivo* study of the antitumor effects of 3′-sulfoquinovosyl-1′-monoacylglycerol (SQMG). Human tumor cells (10^6) of the cell lines (a) MDA-MB-231, (b) A549, (c) WiDr, (d) SAS, (e) PC-3, (f) TE-8, and (g) LU65 were injected subcutaneously into mice, and when tumors grew to 30–40 mm^3, mice were injected with saline (control), 5 mg/kg (SQMG 5), or 20 mg/kg (SQMG 20) every day for 14 days. The means ± SE of tumor volumes from each group (n = 4/group) are shown. *$P < 0.01$.

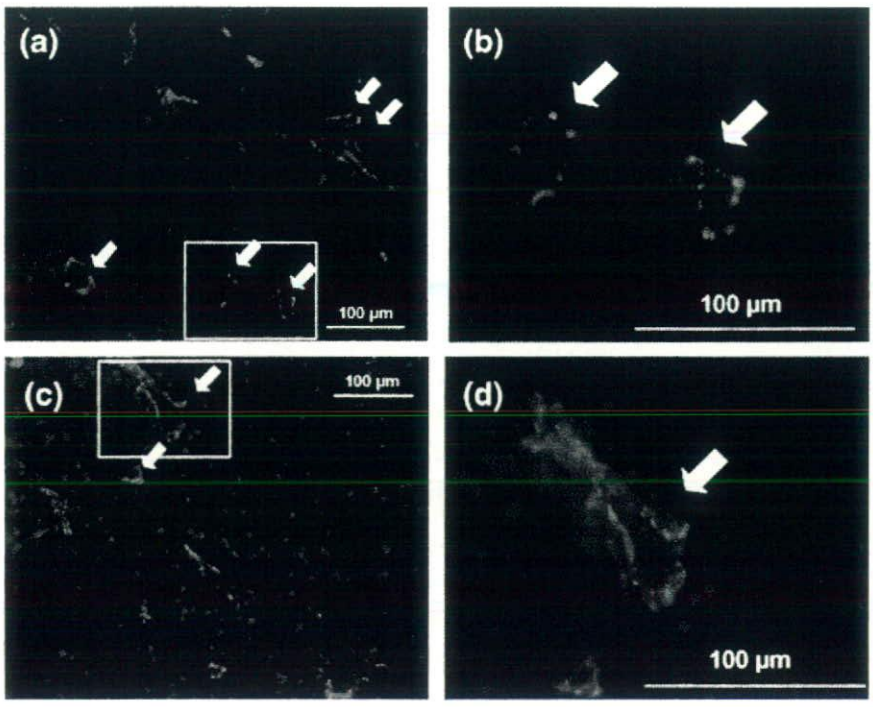

Fig. 3. Antiangiogenesis assessment by immunohistochemical analysis. Cryosections of MDA-MB-231 treated (a,b) without and (c,d) with 3′-sulfoquinovosyl-1′-monoacylglycerol were stained with antimouse CD31 monoclonal antibody and antirat IgG conjugated with AlexaFlour 488, and nuclei were counterstained with propidium iodide. Arrows indicate CD31-positive blood vessels. Insets in (a) and (c) are magnified and shown in (b) and (d), respectively. Scale bar = 100 μm.

cytotoxic potential up to the concentration of 100 μM SQMG (Fig. 4c). Meanwhile, when 50 μM SQMG was added to these cells, capillary network formation was markedly inhibited compared with the control (Fig. 5a–c). Quantitation of these capillary areas by Image ++ software showed that the capillary formation treated with 50 μM SQMG was reduced approximately 70% compared with the control (Fig. 5d). Thus, these data suggest that SQMG could influence capillary formation.

Influence of SQMG on *VEGF* gene expression in tumor tissues. It is known that angiogenesis is basically dependent on VEGF.[1,2] We next quantified the mRNA copy number of tumor-derived $VEGF_{165}$ in mice bearing tumors treated with or without 5 and

doi: 10.1111/j.1349-7006.2008.00785.x

Table 2. Number of tumor-induced blood vessels in tumor tissues

Criteria	Tumor	No. blood vessels (500 mm²)	
		Control	SQMG
Sensitive	MDA-MB-231[†]	10.2 ± 1.0	2.3 ± 1.8*
	A549	6.3 ± 1.1	2.9 ± 0.3*
	WiDr	13.4 ± 4.2	6.6 ± 2.6*
	SAS	15.2 ± 1.3	7.2 ± 1.6*
Resistant	PC-3	10.7 ± 1.7	11.9 ± 2.7
	TE-8	11.4 ± 2.4	11.7 ± 1.9
	LU65	6.2 ± 2.2	3.8 ± 1.1

[†]Data are presented as mean ± SE. *$P < 0.01$. SQMG, 3′-sulfoquinovosyl-1′-monoacylglycerol.

20 mg/kg SQMG by quantitative real-time RT-PCR. *G6PDH* expression was used as a housekeeping gene control. Consequently, as indicated in Table 3, in all four SQMG-sensitive and the three resistant models, the mRNA copy number of human $VEGF_{165}$ did not show any overt difference between controls and SQMG treatment groups, suggesting that SQMG did not influence *VEGF* gene expression. In our preliminary experiments using enzyme-linked immunosorbent assay, VEGF secretion in SQMG-sensitive MDA-MB-231 and SQMG-resistant TE-8 tumor tissues did not differ between controls and SQMG treatment groups (data not shown).

Influence of SQMG on angiopoietin expression in tumor tissues. We next quantified the mRNA copy numbers of *Ang1* and *Ang2*, which are known as important factors for vascular remodeling. Because Ang1 and Ang2 are expressed mainly in pericytes and endothelial cells, respectively,[10] the amounts of their expression in mice were adjusted with the amounts of *G6PDH*-normalized *SM22α* and *CD31*, respectively ([mRNA copy number of target gene/mRNA copy number of G6PDH]/[mRNA copy number of SM22α or CD31/mRNA copy number of G6PDH]).[23] In the SQMG-sensitive tumors MDA-MB-231, A549, and SAS, the mRNA copy numbers of *Ang1* in SQMG-treated tumors appeared to have a tendency to increase two- to three-fold (Table 4), whereas this was not true for *Ang2*.

Downregulation of *Tie2* gene expression in SQMG-sensitive tumors. We demonstrated that although SQMG had less effect on cytotoxic activity against endothelial cells *in vitro* and on VEGF secretion *in vivo*, it strongly inhibited angiogenesis *in vitro* and *in vivo*. To investigate the reasons why the number of mouse-derived blood vessels was decreased by SQMG treatment, we next quantified the mRNA copy numbers of receptor genes related to angiogenesis that are expressed on the endothelial cell surface, namely, *Flt-1*, *Flk-1*, *Tie1*, and *Tie2*, by quantitative real-time RT-PCR. The expression profiles of these genes were calculated with the following formula using the mRNA copy number of each gene, as shown previously:[23]

(target gene/G6PDH)/(CD31/G6PDH).

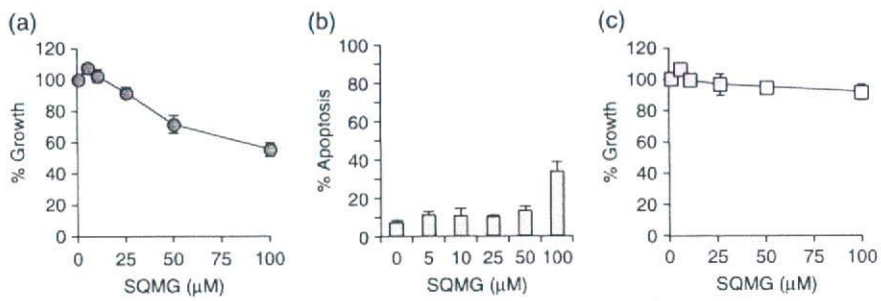

Fig. 4. Influence of 3′-sulfoquinovosyl-1′-monoacylglycerol (SQMG) on cell proliferation and apoptosis. (a) Human umbilical vein endothelial cells (HUVEC) and (c) NIH3T3 were cultured in the presence or absence of SQMG at the indicated concentrations. Cell proliferation was examined by MTT assay. Results represent means ± SE of triplicate wells on one of three independent experiments. (b) HUVEC were cultured in the presence or absence of SQMG at the concentrations indicated for 48 h, harvested, and double-stained with annexin-V–fluorescein and propidium iodide (PI). The percentage of apoptotic (annexin V and PI double positive) cells was determined by flow cytometric analysis. Results represent means ± SE of three independent experiments.

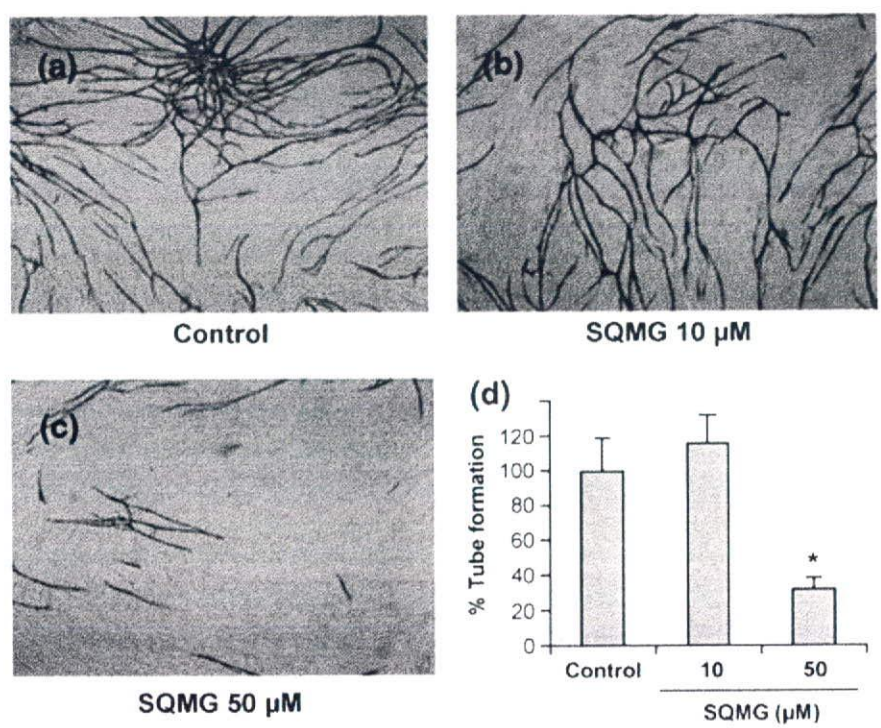

Fig. 5. Effect of 3′-sulfoquinovosyl-1′-monoacylglycerol (SQMG) on angiogenesis *in vitro*. (a–c) Human umbilical vein endothelial cells (HUVEC) grown on a fibroblast sheet on Matrigel were cultured (a) without and (b,c) with SQMG at the indicated concentrations. After cultivation, the cells were fixed and stained with an antihuman CD31 antibody for 1 h. CD31 molecules were detected using the alkaline phosphate method. (d) The tube formation of HUVEC was quantitated using Image ++ software. Results represent means ± SE of five independent areas on one of three independent experiments. *$P < 0.01$.

Table 3. Human vascular endothelial growth factor (*VEGF*) gene expression in tumor tissues treated without or with 3′-sulfoquinovosyl-1′-monoacylglycerol (SQMG)

Criteria	Tumor	mRNA copy number (human $VEGF_{165}$/G6PDH)		
		Control	SQMG-5[1]	SQMG-20[1]
	MDA-MB-231[1]	2.71 ± 0.63	2.76 ± 0.61	2.91 ± 0.81
Sensitive	A549	0.15 ± 0.01	0.21 ± 0.06	0.18 ± 0.03
	WiDr	4.43 ± 0.61	2.40 ± 0.05	2.37 ± 0.42
	SAS	1.89 ± 0.14	1.99 ± 0.04	1.67 ± 0.1
	PC-3	0.58 ± 0.11	0.63 ± 0.04	0.66 ± 0.01
Resistance	TE-8	1.54 ± 0.56	ND	1.76 ± 0.58
	LU65	3.23 ± 0.43	ND	3.25 ± 0.82

[1]Data are presented as mean ± SE. G6PDH, glyceraldehyde-6-phosphate dehydrogenase; ND, not done; SQMG 5, treatment with 5 mg/kg SQMG; SQMG 20, treatment of 20 mg/kg SQMG.

As shown in Table 5, the mRNA copy number of the mouse *Flt-1* gene per copy of the *CD31* gene, which is expressed on mouse endothelial cells in tumor tissues, was similar in controls and after SQMG treatment. This was also true for the mRNA copy number of mouse *Flk-1* in most tumor tissues other than SAS tumors. Only in A549 did *Tie1* gene expression seem to be influenced by SQMG treatment. In contrast, the mRNA copy number of mouse Tie2 in tumor tissues was significantly downregulated in all SQMG-sensitive tumors but not in SQMG-resistant tumors, suggesting that SQMG might affect mouse *Tie2* gene expression in the endothelial cells.

We further investigated whether *Flt-1*, *KDR*, and *Tie2* gene expression in capillary-formed HUVEC were influenced by SQMG *in vitro*. As shown in Figure 6, although *Flt-1* and *KDR* expression were not influenced, *Tie2* gene expression in capillary-formed HUVEC was also downregulated to approximately 50% lower than the control level when 50 μM SQMG was added to cells. Taken together, the data suggest that SQMG plays a role in downregulating *Tie2* gene expression *in vivo* and *in vitro*.

Table 4. Mouse angiopoietin (Ang) gene expression in tumor tissues

Tumor	Treatment	mRNA copy number ratio	
		Ang-1/SM22α	Ang-2/CD31
	Control	0.045 ± 0.015	0.158 ± 0.053
MDA-MB-231	SQMG 5	0.187 ± 0.095*	0.312 ± 0.078
	SQMG 20	0.120 ± 0.047*	0.300 ± 0.103
	Control	0.028 ± 0.003	1.838 ± 1.087
A549	SQMG 5	0.041 ± 0.008*	1.422 ± 0.746
	SQMG 20	0.054 ± 0.028*	4.346 ± 5.406
	Control	0.021 ± 0.001	0.400 ± 0.021
WiDr	SQMG 5	0.017 ± 0.002	0.409 ± 0.053
	SQMG 20	0.022 ± 0.005	0.458 ± 0.059
	Control	0.035 ± 0.025	0.355 ± 0.167
SAS	SQMG 5	0.093 ± 0.047*	0.390 ± 0.185
	SQMG 20	0.091 ± 0.051*	0.448 ± 0.109
	Control	0.008 ± 0.001	0.228 ± 0.067
TE-8	SQMG 5	ND	ND
	SQMG 20	0.009 ± 0.001	0.182 ± 0.100
	Control	0.008 ± 0.001	0.237 ± 0.184
LU65	SQMG 5	ND	ND
	SQMG 20	0.011 ± 0.001	0.225 ± 0.046
	Control	0.572 ± 0.212	0.295 ± 0.054
PC-3	SQMG 5	0.172 ± 0.024	0.340 ± 0.176
	SQMG 20	0.301 ± 0.077	0.392 ± 0.040

*P-values are in the range of 0.22–0.54.
Data are presented as mean ± SE. ND, not done; SQMG 5, treatment of 5 mg/kg SQMG; SQMG 20, treatment of 20 mg/kg SQMG.

Discussion

In the present study, we demonstrated that SQMG induced anti-angiogenic effects in tumor xenografts, resulting in inhibition of solid tumor growth. As significant decreases in tumor angiogenesis were observed in SQMG-sensitive tumors but not in SQMG-resistant tumors, it was speculated that the antitumor

Table 5. Angiogenic receptor gene expression on mouse endothelial cells in tumors

Tumor	Treatment	mRNA copy number ratio (target gene/*CD31* gene)			
		Flt-1	Flk-1	Tie1	Tie2
	Control	0.22 ± 0.02	0.80 ± 0.07	0.56 ± 0.10	0.10 ± 0.01
MDA-MB-231	SQMG 5	0.22 ± 0.02	0.82 ± 0.06	0.59 ± 0.06	0.07 ± 0.01
	SQMG 20	0.26 ± 0.04	0.69 ± 0.06	0.64 ± 0.01	0.06 ± 0.02**
	Control	0.21 ± 0.01	0.82 ± 0.02	0.64 ± 0.09	0.20 ± 0.01
A549	SQMG 5	0.20 ± 0.01	0.67 ± 0.02	0.58 ± 0.10	0.08 ± 0.01**
	SQMG 20	0.24 ± 0.01	0.79 ± 0.01	1.21 ± 0.38*	0.14 ± 0.012*
	Control	0.33 ± 0.02	0.69 ± 0.02	0.58 ± 0.03	0.08 ± 0.01
WiDr	SQMG 5	0.31 ± 0.03	0.64 ± 0.01	0.59 ± 0.02	0.07 ± 0.01
	SQMG 20	0.33 ± 0.01	0.64 ± 0.02	0.63 ± 0.02	0.06 ± 0.01*
	Control	0.36 ± 0.01	1.04 ± 0.02	1.96 ± 0.58	0.20 ± 0.01
SAS	SQMG 5	0.35 ± 0.02	0.93 ± 0.05	2.16 ± 0.73	0.18 ± 0.01
	SQMG 20	0.25 ± 0.01	0.52 ± 0.03**	1.94 ± 0.43	0.11 ± 0.01**
	Control	0.16 ± 0.01	0.93 ± 0.02	1.42 ± 0.03	0.08 ± 0.01
PC-3	SQMG 5	0.11 ± 0.13	0.73 ± 0.06	1.26 ± 0.17	0.07 ± 0.05
	SQMG 20	0.15 ± 0.02	0.78 ± 0.07	1.40 ± 0.04	0.09 ± 0.01
	Control	0.34 ± 0.03	0.74 ± 0.05	0.43 ± 0.11	0.08 ± 0.01
TE-8	SQMG 5	ND	ND	ND	ND
	SQMG 20	0.30 ± 0.02	0.70 ± 0.04	0.44 ± 0.11	0.10 ± 0.01
	Control	0.23 ± 0.02	0.55 ± 0.06	0.43 ± 0.01	0.04 ± 0.01
LU65	SQMG 5	ND	ND	ND	ND
	SQMG 20	0.21 ± 0.21	0.69 ± 0.01	0.42 ± 0.02	0.04 ± 0.01

Data are presented as mean ± SE. ND, not done; SQMG 5, treatment of 5 mg/kg SQMG; SQMG 20, treatment of 20 mg/kg SQMG.
*$P < 0.05$. **$P < 0.01$.

doi: 10.1111/j.1349-7006.2008.00785.x

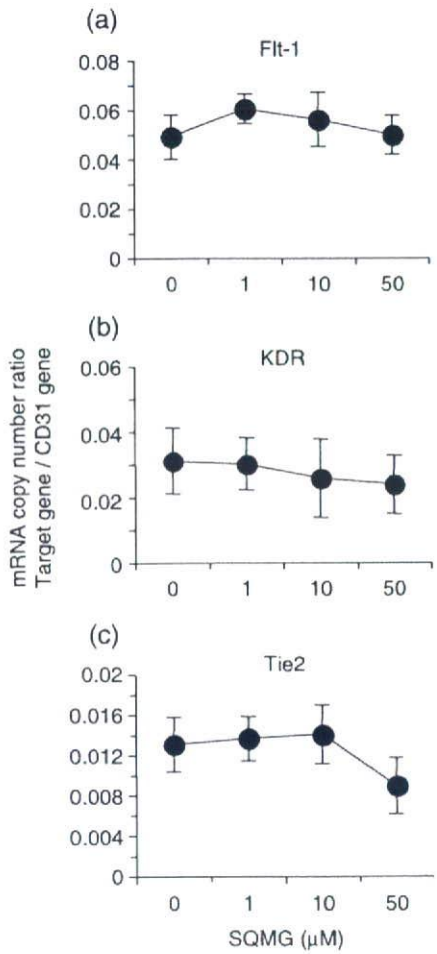

Fig. 6. Angiogenic receptor gene expression on capillary-formed human umbilical vein endothelial cells (HUVEC) *in vitro*. Total RNA of capillary-formed HUVEC was assessed as to the amount of mRNA copy number of human (a) *Flt-1*, (b) *KDR*, and (c) *Tie2* by quantitative real-time reverse transcription–polymerase chain reaction analysis. Results represent means ± SE of triplicate wells on one of three independent experiments.

effects of SQMG could be attributed to the inhibition of tumor angiogenesis. To analyze this mechanism, we first investigated the influence of endothelial cell proliferation and apoptosis *in vitro* by SQMG. Although the proliferation of HUVEC cells treated with 50 μM SQMG was inhibited, the apoptosis of these cells were not clearly observed. Consequently, our study implied that the inhibitory effects of SQMG shown in the MTT assay are attributed to a slower proliferation of HUVEC cells but not apoptosis.

Thus, SQMG appears to have only a weak inhibitory effect on cell proliferation and apoptosis activity as compared with other chemotherapeutic compounds for cancer.[24,25] However, the capillary formation, consisting of HUVEC treated with 50 μM SQMG, was significantly reduced approximately 70% as compared with the control. As *Tie2* but not *Flt-1* and *KDR* gene expression in capillary-formed HUVEC was decreased selectively, it is possible that some synergistic effects between slow proliferation and downregulation of *Tie2* gene expression exist. This was comparable with our observation that xenografted tumors treated with SQMG showed downregulation of *Tie2* gene expression in the endothelial cells. In addition, we recently found that the SQMG-derivative α-SQMG (c18:0) binds to the extracelluar domains of Tie2 using phage display screening and surface plasmon resonance analysis (Sakimoto I, Ohta K, Yamazaki T, *et al.* 2006 unpublished data in Discussion of[21]). Such binding may influence antiangiogenesis through downregulation of Tie2.

The receptor tyrosine kinase Tie2 is highly expressed in endothelial cells, and plays a critical role in normal vascular development via the regulation of vascular remodeling and endothelial cell interactions with supporting pericytes and smooth muscle cells.[26–32] In particular, Tie2 is essential for the development of embryonic vasculature but not hematopoietic cell development[33] because *Tie2*$^{-/-}$ mice die between embryonic days 9.5 and 12.5 due to lack of remodeling of the primary capillary plexus.[28,29] However, Tie2 is constitutively expressed and phosphorylated at a low level in adult mice, suggesting that Tie2 activation is required in adult tissue to maintain the mature quiescent phenotype of vasculature.[34] Interruption of Tie2 signaling with a soluble receptor can significantly inhibit tumor growth in mice, suggesting that Tie2 is important for tumor angiogenesis as well.[11] However, the molecular mechanism by which SQMG induces the downregulation of *Tie2* gene expression *in vivo* and *in vitro* was not demonstrated. The regulatory mechanism of *Tie2* gene expression by SQMG is currently under investigations.

We also observed increased *Ang1* gene expression in three of the four SQMG-sensitive tumors. Ang1 and Ang2 are known to function as ligands for Tie2. Ang1, mainly secreted from pericytes, acts as an agonist of Tie2, whereas Ang2, mainly secreted from endothelial cells, is known to act as an antagonist as well as an agonist, depending on the experimental system.[10] Ang1 specifically induces tyrosine phosphorylation of Tie2, which results in multiple activities related to angiogenesis such as endothelial cell migration,[35] tube formation,[15] sprouting,[36,37] and survival[38,39] but not proliferation of endothelial cells *in vitro*.[40] Thus, Ang1 basically act as a factor of angiogenesis. However, it was reported that Ang1-overexpressing human tumor xenografts could not grow due to inhibition of angiogenesis,[41,42] proposing an inhibitory mechanism whereby the antiangiogenic effects of Ang1 overexpression are mediated in part by increased support by vascular pericytes that results in overall vessel stabilization and therefore inhibition of the initiation of tumor angiogenesis. In the current study, although an upregulation of Ang1 in SQMG-treated tumor xenograft was observed, it remains undefined whether Tie2 phosphorylation levels were influenced by SQMG. The further regulatory mechanism of antiangiogenesis between the Ang1 and Tie2 molecules and how SQMG regulates this needs further study.

In conclusion, as little is known about chemical compounds inducing downregulation of Tie2, SQMG could be a promising candidate for the treatment of tumor-induced angiogenesis targeting Tie2.

Acknowledgments

This research was supported by The Special Coordination Funds on Science and Technology of the Ministry of Education, Culture, Sports, Science of Japan and a research grant from Toyo Suisan.

References

1 Folkman J. What is the evidence that tumor are angiogenesis dependent? *J Natl Cancer Inst* 1990; **82**: 4–6.
2 Carmeliet P. Angiogenesis in life, disease and medicine. *Nature* 2005; **438**: 932–6.
3 O'Reilly MS, Holmgren L, Shing Y *et al.* Angiostatin: a novel angiogenesis inhibitor that mediates the suppression of metastases by a Lewis lung carcinoma. *Cell* 1994; **79**: 315–28.